Absorption band structure of the photochromic dimethyldihydropyrene/metacyclophanediene couple. Insight from vibronic coupling theory

Rudraditya Sarkar, Marie-Catherine Heitz, Martial Boggio-Pasqua

The Journal of Chemical Physics

Absorption band structure of the photochromic dimethyldihydropyrene/metacyclophanediene couple. Insight from vibronic coupling theory

Cite as: J. Chem. Phys. **157**, 224303 (2022); https://doi.org/10.1063/5.0125114
Submitted: 09 September 2022 • Accepted: 18 November 2022 • Accepted Manuscript Online: 21 November 2022 • Published Online: 09 December 2022

Rudraditya Sarkar, Marie-Catherine Heitz and Martial Boggio-Pasqua

The Journal of Chemical Physics ARTICLE scitation.org/journal/jcp

Absorption band structure of the photochromic dimethyldihydropyrene/metacyclophanediene couple. Insight from vibronic coupling theory

Cite as: J. Chem. Phys. 157, 224303 (2022); doi: 10.1063/5.0125114
Submitted: 9 September 2022 • Accepted: 18 November 2022 •
Published Online: 9 December 2022

Rudraditya Sarkar,[1,2,a)] Marie-Catherine Heitz,[1] and Martial Boggio-Pasqua[1,a)]

AFFILIATIONS

[1] Laboratoire de Chimie et Physique Quantiques (UMR 5626), CNRS et Université de Toulouse 3, 31062 Toulouse, France
[2] Institut de Química Computacional i Catàlisi and Department de Química, Universitat de Girona, 17003 Girona, Catalonia, Spain

[a)] **Authors to whom correspondence should be addressed:** rudra.smgr@gmail.com and martial.boggio@irsamc.ups-tlse.fr

ABSTRACT

A detailed insight behind the structure of absorption bands of the photochromic couple dimethyldihydropyrene (DHP)/metacyclophanediene (CPD) is studied employing vibronic coupling theory. Two separate model molecular Hamiltonians, including a maximum of four electronic states and 18 vibrational modes for DHP and five electronic states and 20 vibrational modes for CPD, are constructed in a diabatic electronic representation. The parameters of the Hamiltonians are estimated from the electronic energies obtained from extensive density functional theory (DFT) and time-dependent DFT calculations. Based on these Hamiltonians' parameters, a detailed analysis of potential energy curves is performed in conjunction with positional and energetic locations of several stationary points in multi-dimensional potential energy surfaces. Based on the results of electronic structure calculations, quantum nuclear dynamics studies on the electronic excited states of DHP and CPD are performed to understand the impact of non-adiabatic effects on the formation of vibronic structures of absorption bands of these photo-isomers.

I. INTRODUCTION

Dimethyldihydropyrene (DHP) and metacyclophanediene (CPD) represent a negative photochromic couple. In the presence of visible light, DHP converts to CPD and the reverse isomerization occurs under UV irradiation and also thermally[1] (see Fig. 1). The presence of extended π-conjugation makes the electronic excitation of DHP less energetic, while its aromaticity (14 π electrons) and planarity make its ground state energetically the most stable of this photochromic couple. On the other hand, the loss of π-conjugation and aromaticity (16 π-electrons) makes CPD a less stable isomer and its electronic excitation requires higher energies.[2,3] In general, it is found that the change of color upon irradiation of these types of photo-isomers is accompanied by a change of their electronic structure and physical characteristics, such as luminescence,[4,5] magnetism,[6] conductivity,[7,8] and wettability.[9,10] The photochromic property of DHP and its derivatives upon exposure to visible light follows the timely applications on photo-controlled molecular memories and switches. The present DHP/CPD photochromic couple has unfavorable low photoisomerization quantum yields.[11–16] Therefore, most of the experimental and theoretical investigations[16–27] are focused on the synthesis and design of more efficiently substituted DHPs for usable photo-controlled molecular memories and switches operating at low excitation energies. As a result, a wide range of derivatives of DHP have been synthesized and their photoisomerization quantum yields have been measured employing absorption and fluorescence spectroscopy. The analysis of the absorption spectra of DHPs indicates well-separated bands, whereas, for CPDs, a complex and congested broad band structure is observed.[3,16–18] The above discussions indicate the presence of a wealth of literature studies[11–18,20–22] regarding the explanation of the low quantum yields of the DHP to CPD photoisomerization, while the proper rationalization of the UV–vis band structure of DHPs and CPDs is largely missing in the literature since their first synthesis.[1–3] The goal of this article is to present the details of the UV–vis band structure of the unsubstituted DHP

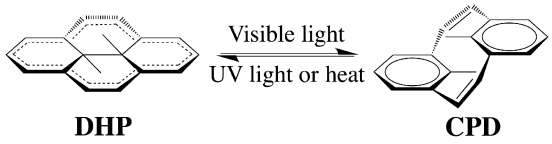

FIG. 1. Schematic representation of the photochromic transformation from DHP to CPD and vice versa.

and CPD on the light of the well-established vibronic coupling (VC) theory.[28–34]

The lowest energy band of DHP,[3] acetyl and acetylene substituted DHPs,[16] benzyl, naphthyl, and anthrayl substituted DHPs,[17] and other substituted DHPs reported in Ref. 35 was observed near ~650 nm with a low molar absorptivity. It was also found that the absorption spectra of DHPs in the 200–700 nm range consist of four distinct bands. Although, depending on the substitutions, the positions and absorptivity of these bands are slightly changed, the overall structure remained unchanged. Similar analyses of the CPDs from the above-mentioned references indicate an obvious blue shift of the overall absorption band of CPDs as compared to DHPs due to the loss of conjugation in the annulene ring. The striking difference between the absorption spectra of these photo-isomers is the existence of a broad band structure for CPDs, while the spectra of DHPs contain individual and well-separated absorption bands. From the theoretical point of view, previous studies on DHP/CPD photo-isomerism[21,22,36] indicate the existence of four well-separated bright singly excited electronic states for DHP ($1^1\tilde{A}_u$, $1^1\tilde{B}_u$, $2^1\tilde{A}_u$, and $2^1\tilde{B}_u$), while for CPD, among the first five excited states, three singly excited states ($1^1\tilde{B}_u$, $1^1\tilde{A}_u$, and $2^1\tilde{B}_u$) are bright and two other singly excited states ($1^1\tilde{B}_g$ and $2^1\tilde{B}_g$) are optically dark. It was found that the first optically bright singly excited state ($1^1\tilde{B}_u$) of CPD possesses a quite close vertical excitation as compared to the $1^1\tilde{B}_g$ and $2^1\tilde{B}_g$ dark excited states. In other words, the excited states of CPD clearly form two sets of energetically close electronic excited states: a first set consisting of the $1^1\tilde{B}_u$, $1^1\tilde{B}_g$, and $2^1\tilde{B}_g$ states and the other set consisting of the $1^1\tilde{A}_u$ and $2^1\tilde{B}_u$ states. Therefore, one could speculate that there would be some vibronic coupling between the bright $1^1\tilde{B}_u$ state and the optically dark states ($1^1\tilde{B}_g$ and $2^1\tilde{B}_g$) through a_u ($B_u \otimes B_g$) symmetry vibrational modes. Similarly, the existence of vibronic coupling between the $1^1\tilde{A}_u$ and $2^1\tilde{B}_u$ bright states could be observed through b_g ($A_u \otimes B_u$) symmetry vibrational modes. The above discussion reveals that non-adiabatic effects might play a significant role in the absorption spectra of CPDs, while this is less likely for DHPs.

A benchmark study on the vertical excitations of DHP, model-DHP, CPD, and model-CPD, together with Franck–Condon (FC) absorption spectral simulations of the DHP, model-DHP, and model-CPD, was performed in our previous study.[36] The so-called model systems consist in a simplification of the experimentally used systems obtained by replacing the central methyl groups by hydrogen atoms (aka, dihydropyrene). FC simulations on DHP reproduced its experimental band positions and intensity, while the same on CPD could not be performed as the geometry of the excited states of CPD is quite different from its ground state energy minimum structure and also because the geometries of the excited states of CPD lose their C_{2h} symmetry upon excitation. Therefore, we choose VC theory[28–34] coupled to quantum nuclear dynamics with the multiconfiguration time-dependent Hartree (MCTDH)[37–42] method in order to understand the absorption band structure of DHP and CPD. The advantage of the VC theory is that the ground state equilibrium structure of DHP and CPD can be taken as reference configurations and the electronic structures of the excited states can be predicted based on single point (SP) excitation energy calculations at the distorted geometries of the reference state. There is no need to calculate computationally demanding Hessians of the excited states. It also turned out from our previous investigations[36] that the extended multi-configuration quasi-degenerate perturbation theory (XMCQDPT2) is the most reliable quantum-chemistry method to deal with both single and double excitations, while the third-order variant of the algebraic diagrammatic construction (ADC) and time-dependent density functional theory (TD-DFT) estimate reasonably good single excitation energies of the present photochromic couple. We have considered the first four and the first five singly excited electronic states of DHP and CPD, respectively, in the present study. Therefore, in order to reduce the computational effort, we employ the TD-DFT quantum-chemistry method to evaluate the SP excitation energies needed for the estimation of the parameters of the constructed vibronic Hamiltonians. Finally, using those Hamiltonians' parameters, nuclear dynamics studies are performed in order to analyze the band structure of the absorption spectra of the DHP/CPD photochromic couple.

II. THEORETICAL METHODOLOGY AND COMPUTATIONAL DETAILS

A. Vibronic Hamiltonian

The present study deals with the nuclear dynamics on the first four and first five low-lying excited electronic states of DHP and CPD, respectively. Both isomers belong to the C_{2h} point group in their ground state ($1^1\tilde{A}_g$) energy minimized structure, and these structures are treated as a reference in the present study for the construction of molecular Hamiltonians. The symmetry of the first four excited states of DHP is $1^1\tilde{A}_u$, $1^1\tilde{B}_u$, $2^1\tilde{A}_u$, and $2^1\tilde{B}_u$ in the increasing order of vertical excitation energy (VEE) at its ground state minimum. The symmetry of the first five excited states of CPD is $1^1\tilde{B}_u$, $1^1\tilde{B}_g$, $2^1\tilde{B}_g$, $1^1\tilde{A}_u$, and $2^1\tilde{B}_u$ in the increasing order of VEE at its ground state minimum. Both isomers have 96 normal vibrational modes whose representation can be decomposed as follows:

$$\Gamma = 27a_g \oplus 21b_g \oplus 22a_u \oplus 26b_u. \tag{1}$$

The molecular Hamiltonians for the present calculations are constructed in a diabatic electronic representation, as described by Köppel *et al.*,[28] and the elements of the potential energy matrix are expanded in Taylor's series along the rectilinear dimensionless normal coordinates at the FC geometry. The molecular Hamiltonian, rather the vibronic Hamiltonian, can be written in the following form:

$$\mathcal{H} = \mathcal{H}_0\mathbf{1} + \Delta\mathcal{H}, \tag{2}$$

where $\mathcal{H}$ and $\mathcal{H}_0$ represent the overall molecular Hamiltonian and the Hamiltonian for the reference state, while $\Delta\mathcal{H}$ represents the

Hamiltonian, which takes care of the molecular change after excitation. **1** stands for an unit matrix whose dimension depends on the number of considered electronic states. Thus, it is a 4 × 4 and 5 × 5 unit matrix, respectively, for DHP and CPD. Within the harmonic approximation, the Hamiltonian for the reference state can be written as

$$\mathcal{H}_0 = -\frac{1}{2}\sum_{i=a_g,b_g,a_u,b_u}\omega_i\left(\frac{\partial^2}{\partial Q_i^2}\right) + \frac{1}{2}\sum_{i=a_g,b_g,a_u,b_u}\omega_i Q_i^2, \tag{3}$$

where i indicates the normal vibrational mode and Q_i and ω_i represent the normal coordinate and frequency of the corresponding normal mode at the reference geometry. The non-vanishing elements of the $\Delta\mathcal{H}$ matrix of Eq. (2) are determined using standard vibronic selection rules, as described in Refs. 28–34, and the elements of this matrix can be written after Taylor's expansion,

$$\Delta\mathcal{H}_{kj} = \begin{cases} E_k^0 + \sum_{i=a_g}\kappa_i^k Q_i + \frac{1}{2!}\sum_{i=a_g,b_g,a_u,b_u}\gamma_i^k Q_i^2 & \\ +\sum_{i=a_g} C_i^k Q_i^3 + \sum_{i=a_g,b_g,a_u,b_u} D_i^k Q_i^4 + \cdots & \text{if } k = j, \\ \sum_i \lambda_i^{k-j} Q_i & \text{if } k \neq j, \end{cases} \tag{4}$$

where k and j are electronic state indices. The VEE is represented by E_k^0, whereas the first-order intrastate and interstate coupling following the linear vibronic coupling scheme is represented by κ_i^k and λ_i^{k-j}, respectively. The diagonal elements of $\Delta\mathcal{H}$ are expanded to higher-order Taylor series, including systematically quadratic terms, and up to sixth order terms in some cases. The largest model Hamiltonians constructed in the present study consist of four coupled electronic states and 18 vibrational modes for DHP and five coupled electronic states and 20 vibrational modes for CPD. The choice of vibrational modes is made by considering their excitation strength, which is discussed later in the text.

At this point, it is necessary to discuss about the detailed participation of the vibrational modes depending on their symmetry in the diabatic Hamiltonian presented in Eq. (4). The involvement of the vibrational modes can be obtained from the well-known vibronic selection rule presented in many literature studies.[28–34] The vibronic selection rule states that the symmetrized direct product of the coupling vibrational mode(s) and electronic states should produce a totally symmetric irreducible representation (irrep); in this case, it is A_g. In other words, the direct product of two electronic states should be the same as the symmetry of the direct product of the participated vibrational mode(s). This can be represented in terms of group theory in the following forms:

$$\begin{cases} \Gamma_j \otimes \Gamma_i \otimes \Gamma_m \otimes \cdots \otimes \Gamma_k \supset \Gamma_{A_g} \\ \text{or} \quad \Gamma_j \otimes \Gamma_k \supset \Gamma_i \otimes \Gamma_m \otimes \cdots, \end{cases} \tag{5}$$

where we have previously defined the meaning of indices i, j, and k. Additionally, we indicate that the index of m also defines the vibrational mode. Let us first discuss about the diagonal elements of the Hamiltonian presented in Eq. (4), where only one electronic state is participating (i.e., intrastate coupling). Hence, in this case, indices j and k are the same. The direct product of the two same symmetry states always produces a totally symmetric irrep. Therefore, the irrep of the participating vibrational mode(s) should be totally symmetric [see Eq. (5)]. Similarly, one can see that the totally symmetric vibrational mode(s) appear in the odd-order and all vibrational modes appear in the even-order positions in the diagonal elements in Eq. (4). We explain this in the following way:

$$\begin{cases} \text{first-order,} \\ \Gamma_i \supset a_g, \\ \Gamma_i \not\supset a_u, b_g, b_u, \\ \text{second-order,} \\ \Gamma_i \otimes \Gamma_i \supset a_g, a_u, b_g, b_u, \\ \text{third-order,} \\ \Gamma_i \otimes \Gamma_i \otimes \Gamma_i \supset a_g, \\ \Gamma_i \otimes \Gamma_i \otimes \Gamma_i \not\supset a_u, b_g, b_u, \\ \ldots. \end{cases} \tag{6}$$

Let us now consider the coupling between different states (i.e., interstate coupling), which can be found in the off-diagonal elements of Eq. (4). We explain this by considering the coupling between B_g (j) and B_u (k) symmetric states using Eq. (5),

$$\begin{cases} \Gamma_{B_g} \otimes \Gamma_{B_u} \supset A_u, \\ \text{so,} \quad \Gamma_i \supset a_u. \end{cases} \tag{7}$$

The vibrational modes responsible for the interstate couplings between the other electronic states are determined by following the similar type of formulation mentioned in Eq. (7).

B. Quantum dynamics

The quantum dynamical calculations are performed within the MCTDH framework[37–41] as implemented in the Heidelberg MCTDH package[42] using both time-dependent (TD) and time-independent (TI) formalisms. The TD Schrödinger equation is solved by expressing the wavefunction as a sum of products of single particle functions (SPFs) $\{\varphi_{j_k}{}^{(k)}\}$ in the MCTDH formalism.[43,44] The wavepacket (WP) is expressed as follows:

$$\begin{aligned} \Psi(Q_1,\ldots,Q_f,t) &\equiv \Psi(q_1,\ldots,q_p,t) \\ &= \sum_{j_1}^{n_1}\cdots\sum_{j_p}^{n_p} A_{j_1,\ldots,j_p}(t)\prod_{k=1}^{p}\varphi_{j_k}^{(k)}(q_k,t) \\ &= \sum_J A_J \Phi_J, \end{aligned} \tag{8}$$

where $\Psi(Q_1,\ldots,Q_f,t)$ represents the wavefunction in f degrees of freedom and $\Psi(q_1,\ldots,q_p,t)$ is the wavefunction in p combined modes (MCTDH particles) with $p < f$. Later, $\Psi(q_1,\ldots,q_p,t)$ is expanded as the product of time-dependent MCTDH coefficients $(A_J \equiv A_{j_1,\ldots,j_p})$ and orthonormal TD SPFs. The quantity Φ_J, at the third line of Eq. (8), represents the product of SPFs, termed as Hartree product. The TD SPFs are again expanded in TI primitive basis functions. The Hermite discrete variable representation

is employed for the construction of the primitive basis. The number of SPFs (n_k) is chosen in a way that it always maintains a proper balance between the two limiting cases being the time-dependent-Hartree and the standard method (i.e., propagating a WP on the primitive basis). In this way, a proper correlation between the interacting particles is introduced in our calculations.

The equation of motion of MCTDH is derived by using the Dirac–Frenkel variational principle[45,46] based on the nuclear wavefunction given in Eq. (8). This gives the following MCTDH working equations:[37–41]

$$i\dot{A}_J = \sum_L < \Phi_J|H|\Phi_L > A_L, \tag{9}$$

$$i\dot{\varphi}^{(k)} = (1 - P^{(k)})^{-1}(\rho^{(k)})^{-1} < H >^{(k)} \varphi^{(k)}, \tag{10}$$

where the vector notation of the MCTDH coefficient and SPFs is previously defined and $\rho^{(k)}$ and $< H >^{(k)}$ represent the one-particle density matrix and the matrix of mean-field operators, respectively. The MCTDH projector, $P^{(k)}$, ensures that the SPFs stay orthonormal during the propagation. The MCTDH coefficient (A vector) and SPFs (φ vector) are propagated under the constant mean-field integration scheme. We have chosen the default short iterative Lanczos and Bulirsch–Stoer integrators for A and φ vectors, respectively, with variable step sizes. An initial WP pertinent for representing the vibronic ground state of DHP or CPD is vertically promoted to the low-lying bright electronic states of DHP ($1^1\tilde{A}_u$, $1^1\tilde{B}_u$, $2^1\tilde{A}_u$, and $2^1\tilde{B}_u$) and of CPD ($1^1\tilde{B}_u$, $1^1\tilde{A}_u$, and $2^1\tilde{B}_u$), and the WP is then propagated up to 200 fs on the coupled $1^1\tilde{A}_u$–$1^1\tilde{B}_u$–$2^1\tilde{A}_u$–$2^1\tilde{B}_u$ and $1^1\tilde{B}_u$–$1^1\tilde{B}_g$–$2^1\tilde{B}_g$–$1^1\tilde{A}_u$–$2^1\tilde{B}_u$ electronic states of DHP and CPD, respectively. The autocorrelation functions $[C(t) =< \Psi(0)|\Psi(t) >]$ obtained from individual calculations are damped with an exponential function $[\exp(\frac{-t}{\tau_r})]$ and Fourier transformed and oscillator-strength weighted[47] to get an energy value spectrum.

For the TI calculation, the Hermitian Hamiltonian, represented in a direct product of harmonic oscillator (HO) functions of the reference state, is diagonalized using the Lanczos algorithm[48–50] as implemented in MCTDH program module.[42] The stick line spectrum obtained from these calculations is convoluted with Lorentzian functions to get the spectrum envelope. The comparison between the TI and TD calculations is made possible using the following relation:[32]

$$\Gamma[eV] \approx \frac{1.31}{\tau_r[fs]}, \tag{11}$$

where Γ represents the full width at half maximum (FWHM) of the Lorentzian function used in the stick line convolution and τ_r represents the damping factor used in TD calculation as mentioned above.

C. Computational details

1. Electronic structure and vibronic coupling parameters

A benchmark study on the VEEs of both DHP and CPD was performed in our previous article[36] using different wavefunction based quantum chemistry methods and density-based quantum chemistry methods employing different density functionals. These investigations indicated that both ADC(3) and TD-DFT provide a reasonable description of the excited states with single excitation character, whereas the same levels of theory are not suitable for the excited states with significant double excitation character. The accuracy of the VEEs calculated from these levels of theory is within

TABLE I. Important normal vibrational modes (symmetry) and their harmonic frequencies [in cm^{-1} (eV)] at the equilibrium structure of the ground state ($1^1\tilde{A}_g$) of DHP and CPD calculated at the B3LYP/6-311G(d,p) level of theory. These vibrational modes are included in the dynamical calculations of DHP and CPD.

Modes (symmetry)	This work	Modes (symmetry)	This work
DHP		CPD	
$\nu_3(a_g)$	186(0.0231)	$\nu_4(a_g)$	161(0.0199)
$\nu_{11}(a_g)$	337(0.0418)	$\nu_{12}(a_g)$	328(0.0407)
$\nu_{13}(a_g)$	391(0.0485)	$\nu_{15}(a_g)$	453(0.0562)
$\nu_{16}(a_g)$	458(0.0568)	$\nu_{21}(a_g)$	548(0.0679)
$\nu_{21}(a_g)$	563(0.0698)	$\nu_{25}(a_g)$	637(0.0790)
$\nu_{22}(a_g)$	568(0.0704)	$\nu_{35}(a_g)$	824(0.1022)
$\nu_{32}(a_g)$	803(0.0995)	$\nu_{44}(a_g)$	992(0.1229)
$\nu_{41}(a_g)$	956(0.1186)	$\nu_{55}(a_g)$	1214(0.1505)
$\nu_{63}(a_g)$	1366(0.1694)	$\nu_{67}(a_g)$	1458(0.1808)
$\nu_{76}(a_g)$	1539(0.1908)	$\nu_1(b_g)$	81(0.0100)
$\nu_{79}(a_g)$	1599(0.1982)	$\nu_6(b_g)$	207(0.0257)
$\nu_5(b_g)$	251(0.0312)	$\nu_2(a_u)$	86(0.0107)
$\nu_7(b_g)$	261(0.0324)	$\nu_{10}(a_u)$	263(0.0326)
$\nu_9(b_g)$	279(0.0346)	$\nu_{13}(a_u)$	354(0.0439)
$\nu_{28}(b_g)$	743(0.0922)	$\nu_{17}(a_u)$	475(0.0589)
$\nu_{38}(b_g)$	923(0.1145)	$\nu_{43}(a_u)$	990(0.1227)
$\nu_{64}(b_g)$	1365(0.1694)	$\nu_{56}(a_u)$	1221(0.1514)
$\nu_{68}(b_g)$	1453(0.1801)	$\nu_{77}(a_u)$	1595(0.1978)
$\nu_{75}(b_g)$	1533(0.1901)	$\nu_8(b_u)$	239(0.0297)
$\nu_{77}(b_g)$	1575(0.1953)	$\nu_{58}(b_u)$	1230(0.1525)

TABLE II. Vertical excitation energy (in eV) and the corresponding oscillator strength of the first four and first five excited electronic states of DHP and CPD, respectively, using the TD-CAM-B3LYP level of theory and the 6-311G(d,p) basis set.

This work			This work		
DHP			CPD		
State	VEE	f	State	VEE	f
$1^1\tilde{A}_u$	2.1845	0.0021	$1^1\tilde{B}_u$	3.6419	0.0184
$1^1\tilde{B}_u$	2.5788	0.0197	$1^1\tilde{B}_g$	3.7774	0.0000
$2^1\tilde{A}_u$	3.4099	0.2844	$2^1\tilde{B}_g$	3.9528	0.0000
$2^1\tilde{B}_u$	3.8981	0.8559	$1^1\tilde{A}_u$	4.6021	0.0021
			$2^1\tilde{B}_u$	4.8866	0.3564

TABLE III. First-order (κ), second-order (γ), and higher-order (C, D, and F) intrastate coupling parameters (in eV) of the relevant vibrational modes for the $1^1\tilde{A}_u$, $1^1\tilde{B}_u$, $2^1\tilde{A}_u$, and $2^1\tilde{B}_u$ electronic states of DHP. The parameters are evaluated from the calculated TD-CAM-B3LYP/6-311G(d,p) electronic energy data. The numbers given in the parentheses represent the excitation strength of the relevant symmetric vibrational modes. Data corresponding to this table are used in the dynamical calculations of DHP.

Mode	$\kappa_i^j\left(\frac{(\kappa_i^j)^2}{2\omega_i^2}\right)$	γ_i^j	C	D	F (sixth-order)	$\kappa_i^j\left(\frac{(\kappa_i^j)^2}{2\omega_i^2}\right)$	γ_i^j	C	D	F (sixth-order)
		$1^1\tilde{A}_u$					$1^1\tilde{B}_u$			
$\nu_3(a_g)$	−0.0160(0.240)	−0.0040				−0.0273(0.698)	−0.0050			
$\nu_{11}(a_g)$	0.0113(0.037)	−0.0029				0.0123(0.043)	−0.0008			
$\nu_{13}(a_g)$	−0.0352(0.263)	−0.0008				−0.0253(0.136)	−0.0025			
$\nu_{16}(a_g)$	0.0126(0.025)	−0.0045				0.0209(0.068)	−0.0040			
$\nu_{21}(a_g)$	0.0164(0.028)	−0.0017				0.0132(0.018)	−0.0016			
$\nu_{22}(a_g)$	0.0022(0.000)	−0.0149				−0.0295(0.088)	−0.0133			
$\nu_{32}(a_g)$	0.0173(0.015)	−0.0084				0.0063(0.002)	−0.0061			
$\nu_{41}(a_g)$	−0.0198(0.014)	−0.0009				−0.0442(0.069)	−0.0034			
$\nu_{63}(a_g)$	−0.0439(0.034)	−0.0011				−0.0950(0.157)	−0.0124			
$\nu_{76}(a_g)$	0.0050(0.000)	0.0031				−0.0782(0.084)	−0.0196	0.0009		
$\nu_{79}(a_g)$	0.0271(0.009)	0.0064				−0.0673(0.058)	−0.0208	0.0011	0.000 02	
$\nu_5(b_g)$		−0.0080					−0.0070			
$\nu_7(b_g)$		−0.0023					−0.0078			
$\nu_9(b_g)$		−0.0055					−0.0039			
$\nu_{28}(b_g)$		−0.0022					−0.0021			
$\nu_{38}(b_g)$		−0.0109					−0.0043			
$\nu_{64}(b_g)$		−0.0006		−0.000 02			−0.0217		0.000 06	
$\nu_{68}(b_g)$		0.0019		−0.000 03	0.000 002		−0.0347		0.000 23	
$\nu_{75}(b_g)$		0.0017		0.000 34	−0.000 041		−0.0558		0.000 66	
$\nu_{77}(b_g)$		0.0029		0.000 03	−0.000 003		−0.0329		0.000 23	
		$2^1\tilde{A}_u$					$2^1\tilde{B}_u$			
$\nu_3(a_g)$	−0.0159(0.237)	−0.0060				−0.0163(0.249)	−0.0056			
$\nu_{11}(a_g)$	0.0283(0.229)	−0.0014				0.0187(0.100)	−0.0046			
$\nu_{13}(a_g)$	−0.0501(0.534)	−0.0014				−0.0522(0.579)	−0.0001			
$\nu_{16}(a_g)$	0.0003(0.000)	−0.0031				0.0023(0.001)	−0.0059			
$\nu_{21}(a_g)$	0.0074(0.006)	−0.0028				0.0195(0.039)	−0.0022			
$\nu_{22}(a_g)$	−0.0021(0.000)	−0.0151				0.0197(0.039)	−0.0133			
$\nu_{32}(a_g)$	0.0223(0.025)	−0.0116				0.0306(0.047)	−0.0119	−0.000 1		
$\nu_{41}(a_g)$	−0.0265(0.025)	−0.0016				−0.0207(0.015)	−0.0005			
$\nu_{63}(a_g)$	−0.0562(0.055)	−0.0026				−0.0207(0.007)	0.0071	−0.000 18		
$\nu_{76}(a_g)$	−0.0028(0.000)	−0.0001	−0.000 14	−0.000 02		0.0808(0.090)	0.0222			
$\nu_{79}(a_g)$	0.0253(0.008)	0.0002	−0.000 1	−0.000 01		0.1250(0.199)	0.0350	−0.001 1	−0.000 06	
$\nu_5(b_g)$		−0.0059					−0.0084			
$\nu_7(b_g)$		−0.0049					−0.0043			
$\nu_9(b_g)$		−0.0058					−0.0061			
$\nu_{28}(b_g)$		−0.0020					−0.0009			
$\nu_{38}(b_g)$		−0.0096		0.000 04			−0.0123			
$\nu_{64}(b_g)$		0.0122		−0.000 10			−0.0012		0.000 02	
$\nu_{68}(b_g)$		0.0301		−0.000 26			0.0050		0.000 09	
$\nu_{75}(b_g)$		0.0580		−0.001 05	0.000 010		0.0118		0.000 18	
$\nu_{77}(b_g)$		0.0330		−0.000 30			0.0034		0.000 13	

~0.3 eV when compared to the results obtained from the more accurate XMCQDPT2 level of theory. The state ordering and the symmetry of the considered electronic states of DHP were found to be the same using all wavefunction-based methods [CASSCF, CASPT2, MS-CASPT2, NEVPT2, QD-NEVPT2, XMCQDPT2, ADC(2), and ADC(3)] and different DFT functionals (B3LYP, B3PW91, CAM-B3LYP, PBE0, TPSSh, M06 M06-2X, and ωB97XD) used in our previous study.[36] The exception in the state ordering was found between TD-DFT and other wave function-based methods (NEVPT2, QD-NEVPT2, XMCQDPT2, ADC(2), and ADC(3)] for the first two

TABLE IV. First-order (κ), second-order (γ), and higher-order (C, D, and F) intrastate coupling parameters (in eV) of the relevant vibrational modes for the $1^1\tilde{B}_u$, $1^1\tilde{B}_g$, $2^1\tilde{B}_g$, $1^1\tilde{A}_u$, and $2^1\tilde{B}_u$ electronic states of CPD. The parameters are evaluated from the calculated TD-CAM-B3LYP/6-311G(d,p) electronic energy data. The numbers given in the parentheses represent the excitation strength of the relevant symmetric vibrational modes. Data corresponding to this table are used in the dynamical calculations of CPD.

Mode	$\kappa_i^j\left(\frac{(\kappa_i^j)^2}{2\omega_i^2}\right)$	γ_i^j	C	D	F (sixth-order)	$\kappa_i^j\left(\frac{(\kappa_i^j)^2}{2\omega_i^2}\right)$	γ_i^j	C	D	F (sixth-order)
		$1^1\tilde{B}_u$					$1^1\tilde{B}_g$			
$\nu_4(a_g)$	0.1051(13.947)	0.0007				0.0836(8.824)	−0.0031			
$\nu_{12}(a_g)$	0.1437(6.233)	−0.0126				0.0239(0.172)	−0.0059			
$\nu_{15}(a_g)$	0.0266(0.112)	−0.0072				0.0999(1.580)	−0.0092			
$\nu_{21}(a_g)$	−0.1492(2.414)	−0.0081				−0.1285(1.791)	−0.0096			
$\nu_{25}(a_g)$	0.0512(0.210)	−0.0063				0.0482(0.186)	−0.0062			
$\nu_{35}(a_g)$	0.0806(0.311)	−0.0037				0.0009(0.000)	−0.0035	0.001 74	−0.000 38	
$\nu_{44}(a_g)$	0.0313(0.032)	−0.0128	0.000 22	−0.000 09		0.0366(0.044)	−0.0268	0.001 67	0.000 13	
$\nu_{55}(a_g)$	0.0414(0.038)	−0.0033				0.0583(0.075)	−0.0009			
$\nu_{67}(a_g)$	−0.1680(0.432)	−0.0043				−0.0754(0.087)	−0.0066			
$\nu_1(b_g)$		0.0032		−0.000 60			−0.0098		−0.000 17	
$\nu_6(b_g)$		−0.0116					−0.0035			
$\nu_2(a_u)$		0.0003		−0.000 54			−0.0122		−0.000 10	
$\nu_{10}(a_u)$		−0.0321		0.000 20			0.0206		−0.000 99	0.000 040
$\nu_{13}(a_u)$		−0.0257		0.000 14			0.0098		−0.000 52	0.000 020
$\nu_{17}(a_u)$		−0.0788		0.001 38	−0.000 025		0.0715		−0.005 91	0.000 433
$\nu_{43}(a_u)$		−0.0503		0.000 55	−0.000 009		0.0051		−0.000 45	0.000 008
$\nu_{56}(a_u)$		−0.0567		0.001 07	−0.000 019		0.0518		−0.002 36	0.000 103
$\nu_{77}(a_u)$		−0.1609		0.003 31	−0.000 062		0.0509		−0.003 56	0.000 181
$\nu_8(b_u)$		−0.0024					−0.0034			
$\nu_{58}(b_u)$		−0.0058					−0.0123			
		$2^1\tilde{B}_g$					$1^1\tilde{A}_u$			
$\nu_4(a_g)$	0.0829(8.677)	−0.0039				0.0318(1.277)	−0.0039			
$\nu_{12}(a_g)$	0.1172(4.146)	−0.0070				0.0022(0.001)	−0.0080	0.000 21		
$\nu_{15}(a_g)$	0.0021(0.001)	−0.0047				0.0253(0.101)	−0.0113			
$\nu_{21}(a_g)$	−0.0971(1.023)	−0.0082				−0.0517(0.290)	−0.0115			
$\nu_{25}(a_g)$	0.0287(0.066)	−0.0049				−0.0109(0.010)	−0.0024			
$\nu_{35}(a_g)$	0.0779(0.290)	0.0066	−0.000 84			0.0233(0.026)	−0.0037			
$\nu_{44}(a_g)$	0.1011(0.338)	−0.0033	−0.000 75			−0.0001(0.000)	−0.0091	−0.000 13		
$\nu_{55}(a_g)$	0.0796(0.140)	−0.0024				0.0747(0.123)	0.0001			
$\nu_{67}(a_g)$	−0.0977(0.146)	0.0008				−0.0502(0.039)	−0.0039			
$\nu_1(b_g)$		0.0156		−0.000 14	−0.000 009		0.0072		−0.000 30	
$\nu_6(b_g)$		−0.0080					−0.0073			
$\nu_2(a_u)$		0.0131		−0.000 23	−0.000 003		−0.0211		0.001 66	−0.000 076
$\nu_{10}(a_u)$		0.0108		−0.000 03			−0.0065			
$\nu_{13}(a_u)$		0.0101		−0.000 04			−0.0067			
$\nu_{17}(a_u)$		0.0063		0.000 30	−0.000 009		−0.0105			
$\nu_{43}(a_u)$		−0.0030		−0.000 06			−0.0107			
$\nu_{56}(a_u)$		0.0188		−0.000 06			0.0006			
$\nu_{77}(a_u)$		0.0872		−0.001 28			−0.0157		−0.000 23	
$\nu_8(b_u)$		0.0009					0.0024		−0.000 01	
$\nu_{58}(b_u)$		−0.0136		0.000 05			0.0141		−0.000 06	
		$2^1\tilde{B}_u$								
$\nu_4(a_g)$	0.0485(2.970)	−0.0082								
$\nu_{12}(a_g)$	0.0025(0.002)	0.0002								
$\nu_{15}(a_g)$	0.0612(0.593)	−0.0064								
$\nu_{21}(a_g)$	−0.0854(0.791)	−0.0094								
$\nu_{25}(a_g)$	0.0225(0.041)	−0.0048								

TABLE IV. (*Continued*.)

Mode	$\kappa_i^j\left(\frac{(\kappa_i^j)^2}{2\omega_i^2}\right)$	γ_i^j	C	D	F (sixth-order)	$\kappa_i^j\left(\frac{(\kappa_i^j)^2}{2\omega_i^2}\right)$	γ_i^j	C	D	F (sixth-order)
		$2^1\tilde{B}_u$								
$\nu_{35}(a_g)$	0.0097(0.005)	−0.001 1								
$\nu_{44}(a_g)$	0.1035(0.355)	−0.012 9								
$\nu_{55}(a_g)$	0.0914(0.184)	−0.001 2								
$\nu_{67}(a_g)$	−0.003 1(0.000)	−0.0025	−0.000 15							
$\nu_1(b_g)$		−0.003 2		0.000 97	−0.000 053					
$\nu_6(b_g)$		0.061 5		−0.004 56	0.000 110					
$\nu_2(a_u)$		−0.015 5		0.003 35	−0.000 361					
$\nu_{10}(a_u)$		−0.003 8								
$\nu_{13}(a_u)$		−0.002 4								
$\nu_{17}(a_u)$		−0.007 1								
$\nu_{43}(a_u)$		−0.012 9								
$\nu_{56}(a_u)$		0.005 5								
$\nu_{77}(a_u)$		0.027 1		−0.000 14						
$\nu_8(b_u)$		−0.000 02								
$\nu_{58}(b_u)$		−0.022 5		0.000 07						

excited states of CPD. In the following case, the order of these states is reversed although the ordering of these two states is the same for CASPT2 and MS-CASPT2 with all DFT functionals. It was found in our previous study[36] that the absolute errors (in eV) with respect to the available experimental values[16] of the first four excited states of DHP are ~0.02, ~0.20, ~0.19, and ~0.01 obtained from the XMC-QDPT2 level; ~0.30/0.33, ~0.21/0.02, ~0.12/0.04, and ~0.25/0.24 obtained from the ADC(2)/ADC(3) level; and ~0.25, ~0.06, ~0.12, and ~0.23 obtained from the TD-DFT level using the CAM-B3LYP functional. The above discussions indicate that both the ADC(3) and TD-DFT/B3LYP level of theory produce comparable absolute errors for the estimated VEEs of the first four excited states of DHP, while for CPD, to the best of our knowledge, there is no accurate experimental observation of the VEEs of the excited state available. That is why, we rely on the most accurate wavefunction based method: XMCQDPT2, as it estimated most balanced mixing of states than the other considered quantum chemistry methods. The absolute errors (in eV) with respect to the VEEs obtained from the XMCQDPT2 level of theory of the first five excited states of CPD are ~0.27, ~0.25, ~0.26, ~0.34, and ~0.56 obtained from ADC(2); ~0.26, ~0.29, ~0.24, ~0.17, and ~0.79 obtained from ADC(3); and ~0.29, ~0.03, ~0.02, ~0.48, and ~0.47 obtained from the TD-DFT level of theory using the CAM-B3LYP functional. The above discussions indicate that the TD-DFT/CAM-B3LYP level of theory produces a minimum absolute error for the VEEs of the second, third, and fifth excited states, while ADC(3) produces a minimum absolute error for the VEEs of the first and fourth excited states of CPD. On the other hand, we primarily deal with singly excited states of DHP and CPD in the present study. Hence, we have a choice between the two computationally less expensive theories, ADC(2)/ADC(3) and TD-DFT, over the more accurate and more expensive XMCQDPT2. We choose the comparatively less expensive and similarly accurate TD-DFT level of theory over ADC(2)/ADC(3) for our excited state calculations. All DFT and TD-DFT calculations are performed with Gaussian09 program modules.[51]

DFT was employed for both ground and excited state calculations of DHP and CPD using the 6-311G(d,p) basis set. The ground state energy minimum of both DHP and CPD was obtained employing the B3LYP functional,[52] while the confirmation of energy minimum structure was obtained from subsequent analytic frequency calculations at the same level of theory. Relevant harmonic vibrational frequencies at the ground state minimum of DHP and CPD are given in Table I, while a full list of frequencies can be found in Tables SI and SII of the supplementary material. The ground state energy minimum structures of DHP and CPD are treated as references for subsequent SP excited state calculations at the distorted geometries along each normal mode of vibrations of DHP and CPD. The VEEs of the excited states of DHP and CPD at their respective reference geometry are given in Table II in conjunction with their oscillator strengths. The mass-weighted normal displacement coordinates of the vibrational modes are calculated from the eigenvectors of the GF-matrix.[53] These are then transformed to the dimensionless form **Q** by multiplying with the harmonic frequencies (in a.u.).

The VEEs at the distorted geometries (**Q** from −5.00 to +5.00, $\Delta\mathbf{Q}$ = ±0.25, ±0.50, ±1.00, ±1.50, . . ., ±5.00) of DHP and CPD were calculated at the TD-DFT level employing the CAM-B3LYP functional.[54] For these SP energy calculations, we considered all totally symmetric vibrational modes for DHP and CPD, while b_g symmetry coupling modes for DHP and b_g, b_u, and a_u symmetry coupling modes for CPD were considered. Thus, a total of 1056 SP energies and 2112 SP energies for each electronic state were calculated, respectively, for DHP and CPD, in order to estimate the Hamiltonian's parameters. It was discussed in our previous article[36] that the VEEs of DHP were functional independent, while those of CPD were functional dependent. We employ the CAM-B3LYP

TABLE V. Relevant linear interstate coupling parameter (λ^{j-k}) (in eV) and the corresponding excitation strength $\left(\frac{(\lambda^{j-k})^2}{2\omega_i^2}\right)$ between pairs of electronic states j and k of DHP and CPD.

Mode	λ^{j-k}	$\left(\frac{(\lambda^{j-k})^2}{2\omega_i^2}\right)$		λ^{j-k}	$\left(\frac{(\lambda^{j-k})^2}{2\omega_i^2}\right)$
			DHP		
	$1^1\tilde{A}_u$–$1^1\tilde{B}_u$			$1^1\tilde{A}_u$–$2^1\tilde{B}_u$	
$\nu_5(b_g)$	0.0090	0.042	$\nu_{28}(b_g)$	0.0253	0.038
$\nu_9(b_g)$	0.0125	0.065	$\nu_{68}(b_g)$	0.0432	0.029
$\nu_{28}(b_g)$	0.0034	0.004			
$\nu_{38}(b_g)$	0.0253	0.024			
Mode	λ^{j-k}	$\left(\frac{(\lambda^{j-k})^2}{2\omega_i^2}\right)$		λ^{j-k}	$\left(\frac{(\lambda^{j-k})^2}{2\omega_i^2}\right)$
	$1^1\tilde{B}_u$–$2^1\tilde{A}_u$			$2^1\tilde{A}_u$–$2^1\tilde{B}_u$	
$\nu_5(b_g)$	0.0146	0.109	$\nu_7(b_g)$	0.0077	0.028
$\nu_7(b_g)$	0.0256	0.312	$\nu_{28}(b_g)$	0.0104	0.006
$\nu_{28}(b_g)$	0.0072	0.003			
$\nu_{64}(b_g)$	0.0834	0.120			
$\nu_{68}(b_g)$	0.1165	0.209			
$\nu_{75}(b_g)$	0.1462	0.296			
$\nu_{77}(b_g)$	0.1167	0.179			
			CPD		
	$1^1\tilde{B}_u$–$1^1\tilde{B}_g$			$1^1\tilde{B}_u$–$2^1\tilde{B}_g$	
$\nu_{10}(a_u)$	0.0468	1.030	$\nu_2(a_u)$	0.0416	7.558
$\nu_{13}(a_u)$	0.0369	0.353	$\nu_{10}(a_u)$	0.0640	1.927
$\nu_{17}(a_u)$	0.0783	0.884	$\nu_{13}(a_u)$	0.0567	0.834
$\nu_{43}(a_u)$	0.0479	0.076	$\nu_{17}(a_u)$	0.0918	1.215
$\nu_{56}(a_u)$	0.0692	0.104	$\nu_{43}(a_u)$	0.0619	0.127
$\nu_{77}(a_u)$	0.1254	0.201	$\nu_{56}(a_u)$	0.0824	0.148
			$\nu_{77}(a_u)$	0.1793	0.411
	$1^1\tilde{B}_u$–$1^1\tilde{A}_u$			$1^1\tilde{B}_g$–$1^1\tilde{A}_u$	
$\nu_1(b_g)$	0.0503	12.650	$\nu_8(b_u)$	0.0335	0.636
$\nu_6(b_g)$	0.0327	0.809	$\nu_{58}(b_u)$	0.0746	0.120
	$1^1\tilde{B}_g$–$2^1\tilde{B}_u$			$2^1\tilde{B}_g$–$1^1\tilde{A}_u$	
$\nu_2(a_u)$	0.0550	13.211	$\nu_8(b_u)$	0.0151	0.129
			$\nu_{58}(b_u)$	0.0676	0.098
				$1^1\tilde{A}_u$–$2^1\tilde{B}_u$	
			$\nu_1(b_g)$	0.0117	0.684
			$\nu_6(b_g)$	0.0301	0.686

functional for SP TD-DFT calculations of both DHP and CPD in a quest of consistency of the results. Later, these excitation energy values were used for non-linear fitting with the adiabatic analytic form of the potential matrix of Eq. (4) in order to estimate different Hamiltonian's parameters. The intrastate Hamiltonian parameters for DHP are given in Table III, while those for CPD are given in Table IV. Tables III and IV contain the information of the relevant vibrational modes of DHP and CPD included in the dynamics, while data concerning other vibrational modes can be found in Tables SIII and SIV of the supplementary material. The Huang–Rhys parameters $\frac{(\kappa_i^j)^2}{2\omega_i^2}$, defining the excitation strength of the totally symmetric (a_g) vibrational modes, are also given in parentheses in these tables (cf. Tables III and IV). On the other hand, the linear interstate coupling (λ_i^{j-k}) between two electronic states j and k through vibrational mode i can be calculated using the following expression:[28]

$$\lambda_i^{j-k} = \frac{1}{2Q_s}\sqrt{[E_j(Q_s) - E_k(Q_s)]^2 - [E_j(Q_0) - E_k(Q_0)]^2}, \quad (12)$$

where E_j and E_k denote the excitation energy of the jth and kth excited state at the dimensionless normal coordinate Q_s ($Q_s = Q_0 + \Delta Q$) along the normal vibrational modes. ΔQ represents the distortion from the equilibrium ground state reference configuration ($\mathbf{Q_0}$). The calculated values of λ_i^{j-k} for relevant vibrational modes are given in Table V for both DHP and CPD, along with their coupling strength, determined as $\frac{(\lambda^{j-k})^2}{2\omega_i^2}$. The full data of interstate coupling can be found from Tables SV and SVI of the supplementary material, respectively, for DHP and CPD. The choice of non-totally symmetric vibrational modes (b_g, a_u, and b_u) for intrastate coupling is made by considering their respective coupling strength provided in Tables SV and SVI of the supplementary material.

2. Nuclear dynamics

Concerning the WP propagation, the calculations for DHP were performed with 18 vibrational modes listed in Table I (nine totally symmetric and nine non-totally symmetric vibrational modes) and those for CPD were performed with 20 vibrational modes listed in Table I (nine totally symmetric and 11 non-totally symmetric vibrational modes). The methodology and applied integration schemes employed are given in Sec. II B. The normal mode combination and the size of the primitive basis set are given in Table SVII of the supplementary material. The dynamics is initiated by setting the initial WP on the bright electronic states of DHP and CPD, i.e., on the singlet states of A_u and B_u symmetry. A parameter τ_r of 15 fs is used for damping the autocorrelation function, and the oscillator strengths are used for weighting the different spectra.

III. RESULTS AND DISCUSSIONS

A. Potential energy curves

1. Adiabatic potential energy curves along totally symmetric normal coordinates

The detailed topological features of the potential energy curves (PECs) along the relevant normal coordinates are examined in this subsection. PECs along relevant a_g symmetry vibrational modes are shown in Figs. 2 and 3, respectively, for DHP and CPD to illustrate the tuning activity of these modes near the intersections. These

modes combinedly participate in the tuning of the conical intersections (CIs)[55–58] in multidimensional space (see below). The points in Figs. 2 and 3 represent the calculated *ab initio* energy values obtained from the TD-DFT level of theory, and the solid lines are generated from the potential energy part of the model Hamiltonian of Eq. (2) using the respective Hamiltonian parameters of DHP and CPD (cf. Tables I–IV). The superposition of the *ab initio* energy points and the solid lines indicates the quality of the potential fits and acceptability of the constructed model Hamiltonian. For both DHP and CPD, most of the vibrational modes possess significant harmonicity, while some of the vibrational modes show anharmonicity (cf. Tables III and IV and Tables SIII and SIV of the supplementary material). A comparison of the data given in Tables III and IV indicates a stronger Condon activity (defined by Huang–Rhys parameters) of relevant a_g symmetry vibrational modes for CPD than that of DHP. As a result, a comparatively larger shift of energy minimum of the excited electronic states as compared to its ground state (reference state) minimum (at $\mathbf{Q} = 0$) can be observed in Fig. 3 for CPD than for DHP (cf. Fig. 2). In order to illustrate the above comment, we consider the ν_3 and ν_4 vibrational modes of DHP and CPD, respectively, which possess overall the strongest Condon activity. The PECs along these modes are shown in panel (a) of Figs. 2 and 3. The PECs shown in panel (a) of Fig. 2 indicate relatively small shifts of the minima of the four excited states of DHP (~0.84, ~1.52, ~0.94, and ~0.94 unit), while the PECs shown in panel (a) of Fig. 3 indicate rather large shifts of the minima of the five excited states of CPD (~5.10, ~4.98 and ~5.18, ~1.99 and ~4.11 unit). Another noticeable point is that the direction of these positional shifts is guided by the sign of κ for the respective electronic states; a positional shift of the minimum of the excited state occurs in the negative direction in the presence of positive κ and vice versa.[28] The sign of κ for the ν_3 vibrational mode of DHP is negative for all four excited states, while the sign of κ for the ν_4 vibrational mode of CPD is positive for all five excited state. One finds that the position of the minima of the excited states of DHP occurs along the positive direction from its reference state, while the position of the minima of the excited

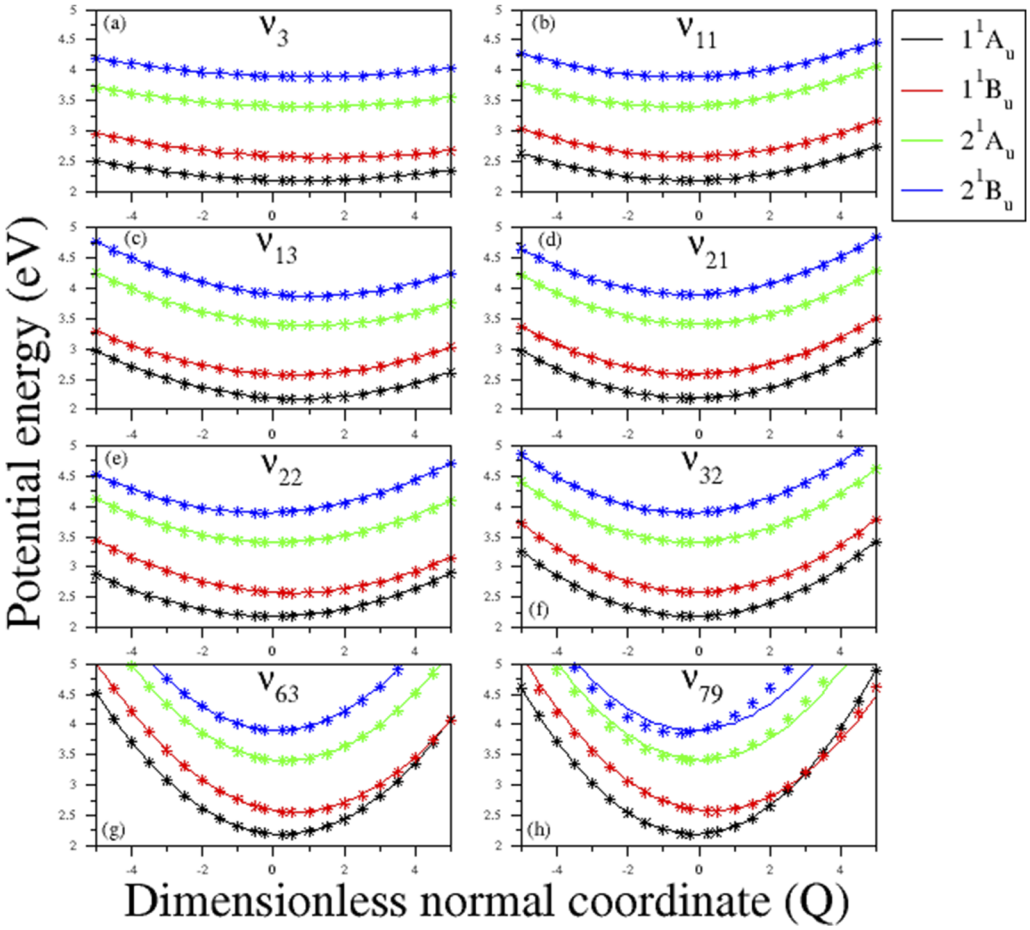

FIG. 2. Potential energy curves (PECs) along some selected totally symmetric (a_g) normal coordinates of DHP. Selection of vibrational modes is performed considering their Poisson parameter $\left[\left(\frac{(\kappa_i^j)^2}{2\omega_i^2}\right)\right]$; see Table III for each electronic state. The PECs along ν_3, ν_{11}, ν_{13}, ν_{21}, ν_{22}, ν_{32}, ν_{63}, and ν_{79} are shown in (a)–(h), respectively.

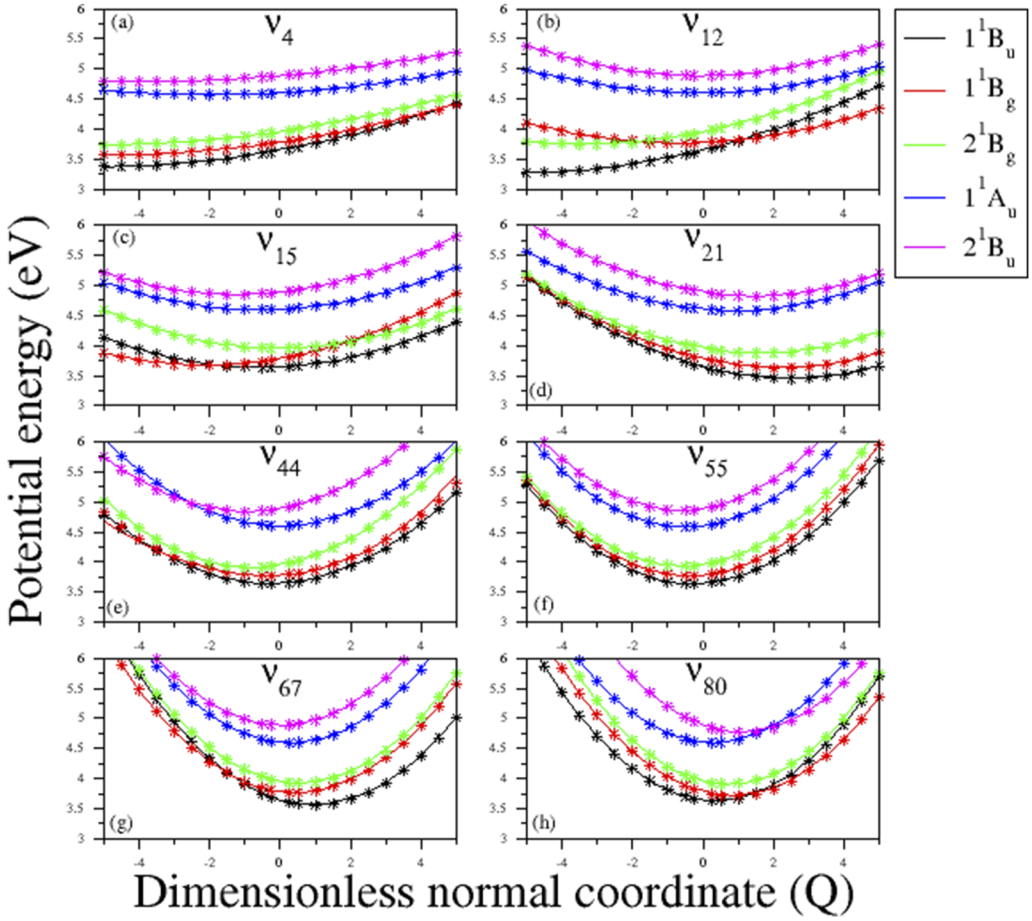

FIG. 3. Potential energy curves (PECs) along some selected totally symmetric (a_g) normal coordinates of CPD. Selection of vibrational modes is performed considering their Poisson parameter $\left[\left(\frac{(\kappa_i^j)^2}{2\omega_i^2}\right)\right]$; see Table IV for each electronic state. The PECs along ν_4, ν_{12}, ν_{15}, ν_{21}, ν_{44}, ν_{55}, ν_{67}, and ν_{80} are shown in (a)–(h), respectively.

states for CPD occurs along the negative direction from its reference state.

The PECs represented in Fig. 2 indicate a significant separation of energies of the $1^1\tilde{A}_u$, $1^1\tilde{B}_u$, $2^1\tilde{A}_u$, and $2^1\tilde{B}_u$ states of DHP at the distorted geometries along Q_3, Q_{11}, Q_{13}, Q_{21}, Q_{22}, and Q_{32} normal coordinates [cf. panels (a)–(f) of Fig. 2]. The scenario is rather different at the distorted geometries along the Q_{63} and Q_{79} normal coordinates. The PECs shown in panels (g) and (h) of Fig. 2 show an intersection between the $1^1\tilde{A}_u$ and $1^1\tilde{B}_u$ states along both normal coordinates, while the other two states ($2^1\tilde{A}_u$ and $2^1\tilde{B}_u$) are well separated. The intersection between the $1^1\tilde{A}_u$ and $1^1\tilde{B}_u$ states along the Q_{63} normal coordinate is quite high in energy. On the other hand, the intersection between the $1^1\tilde{A}_u$ and $1^1\tilde{B}_u$ states along Q_{79} is low in energy. The above discussion indicates that the vibrational modes, ν_{63} and ν_{79}, would play a crucial role in the non-adiabatic phenomena in the nuclear dynamics of the first four excited states of DHP. The diagrammatic representation of the displacement vectors of the normal vibrational modes (included in the dynamics) presented in Table I of DHP is shown in Fig. S1 of the supplementary material. We find that the ν_3, ν_{11}, ν_{22}, and ν_{32} vibrational modes show symmetric bending type vibrations, ν_{13}, ν_{21}, and ν_{79} vibrational modes show symmetric stretching type vibration of the planar pyrene ring, and the ν_{63} vibrational mode shows stretching vibration in the C–CH_3 bonds among the vibrational modes considered in the PECs shown in Fig. 2. This indicates that the stretching motion of C–CH_3 bonds (ν_{63}), one symmetric bending type vibration (ν_{22}), and one breathing vibration (stretching of the pyrene ring), i.e., ν_{79}, plays a more important role in the tuning of energies between the electronic states of DHP.

The situation is more complex for the electronic states of CPD, as indicated in Fig. 3. These PECs clearly indicate two sets of coupled electronic states: the first set consists of the $1^1\tilde{B}_u$, $1^1\tilde{B}_g$, and $2^1\tilde{B}_g$ states and the second set is composed of the $1^1\tilde{A}_u$ and $2^1\tilde{B}_u$ states of CPD. There are several intersections that exist between the $1^1\tilde{B}_u$, $1^1\tilde{B}_g$, and $2^1\tilde{B}_g$ states of CPD, and the energetic locations of these intersections are quite low relative to the energetic minima of these

electronic states. This indicates that the topology of the bright $1^1\tilde{B}_u$ state could be affected by the close lying other two optically dark $1^1\tilde{B}_g$ and $2^1\tilde{B}_g$ states of CPD. On the other hand, fewer intersections can be observed between the $1^1\tilde{A}_u$ and $2^1\tilde{B}_u$ states. In addition, the PECs shown in panels (b), (e), and (h) of Fig. 3 indicate an energetic proximity between the $2^1\tilde{B}_g$ and $1^1\tilde{A}_u$ states. This might also initiate non-adiabatic interactions between the above-mentioned two sets of coupled surfaces. The diagrammatic representation of the displacement vectors of the normal vibrational modes (included in the dynamics) presented in Table I of CPD is shown in Fig. S2 of the supplementary material. We find that the ν_4, ν_{12}, ν_{15}, ν_{21}, ν_{44}, and ν_{55} vibrational modes show symmetric bending type vibrations. Among these symmetric bending type of vibrations, ν_{44} and ν_{55} involved the out-of-plane bending and in-plane bending motion of central moiety, while the ν_{67} and ν_{80} vibrational modes show stretching vibrational motion in the C–CH_3 bond and central moiety, respectively. All these vibrational modes show the tuning activity between the first set of electronic states of CPD as mentioned before, i.e., between the optically bright $1^1\tilde{B}_u$ state and optically dark ($1^1\tilde{B}_g$ and $2^1\tilde{B}_g$) states (see Fig. 3). On the other hand, the tuning activity between the second set of electronic states, i.e., between $1^1\tilde{A}_u$ and $2^1\tilde{B}_u$ states, is prominent along the vibrational modes involved in the either bending (ν_{44}) or stretching (ν_{80}) motion of central moiety, as seen in panels (e) and (h), respectively, of Fig. 3.

The intersections discussed above form CIs in a multidimensional space. The energetic minimum of the seam of various CIs and the equilibrium minimum of electronic states are estimated within a quadratic vibronic coupling model using the parameters of Tables I–IV. The results are given in Table VI for both DHP and CPD. The diagonal and off-diagonal entries of Table VI represent the equilibrium minima of the states and the minima of CI seams, respectively. A constrained minimization by Lagrangian multiplier methods as implemented in the Mathematica software[59] is used to calculate the energetic minimum of the CI seam. The energy minima of the states together with the minima of the CI seams between them govern the mechanistic details of the nuclear dynamics, which will be discussed in Sec. III B 2. Note that it looks like the absolute sign of κ would play a vital role in the nuclear dynamics as the position of the CI between two energetically close lying electronic states with the same sign of κ should be different from the position of the CI of the same electronic states with the opposite sign of κ. The similar argument is true for the position of energy minima of the excited states. However, it is the relative sign of κ with respect to the normal coordinates (Q), which plays a crucial role in the nuclear dynamics.

TABLE VI. Estimated energies of the equilibrium minimum (diagonal entries) and the minimum of the seam of various CIs (off-diagonal entries) of the electronic states of DHP and CPD derived from the quadratic coupling model developed in this paper. The energies are given in eV.

DHP				
	$1^1\tilde{A}_u$	$1^1\tilde{B}_u$	$2^1\tilde{A}_u$	$1^1\tilde{B}_u$
$1^1\tilde{A}_u$	2.1523	2.6191	12.4475	18.1383
$1^1\tilde{B}_u$		2.4697	6.5592	7.3700
$2^1\tilde{A}_u$			3.3518	5.6805
$2^1\tilde{B}_u$				3.8981

CPD					
	$1^1\tilde{B}_u$	$1^1\tilde{B}_g$	$2^1\tilde{B}_g$	$1^1\tilde{A}_u$	$2^1\tilde{B}_u$
$1^1\tilde{B}_u$	2.6705	3.2912	4.2380	5.1070	5.5658
$1^1\tilde{B}_g$		3.2596	3.3706	5.5742	6.5533
$2^1\tilde{B}_g$			3.3321	4.9234	5.5582
$1^1\tilde{A}_u$				4.5104	4.6061
$2^1\tilde{B}_u$					4.6064

2. Impact of non-totally symmetric modes on the PECs

The interstate couplings between two electronic states with different symmetry are mediated through non-totally symmetric vibrational modes. These potential couplings constitute the off-diagonal elements of the diabatic matrix Hamiltonian of Eq. (2). The characterization of the interstate coupling is performed by the dimensionless parameter x_i,[28,60–62] which is defined as $\frac{\lambda^2}{\omega_i\Delta}$, where ω_i is the frequency of the non-totally symmetric vibrational mode i and Δ is the half of the difference between the VEEs of the considered electronic states. The strength of the interstate coupling can be classified as low ($x_i < 1$), moderate ($x_i > 1$), or strong ($x_i \gg 1$). In the present work, inspection of Table V indicates the existence of low interstate couplings in the four excited states of DHP, while moderate to strong interstate couplings exist in the five excited states of CPD. Hence, it is expected that the PECs of the DHP should not be significantly affected by interstate coupling. Considering the existence of strong interstate coupling in CPD, we inspect the effect of these couplings on the close-lying first three coupled excited electronic states ($1^1\tilde{B}_u$, $1^1\tilde{B}_g$, and $2^1\tilde{B}_g$) mediated via the ν_2, ν_{10}, and ν_{17} vibrational modes (Fig. 4). Considering only two states, the adiabatic potential energies along the non-totally symmetric normal coordinate (Q_s) can be written as

$$V_{1,2}(Q_s) = \frac{1}{2}\omega_s {Q_s}^2 + \frac{1}{2}\left[(E_1^0 + E_2^0) + \frac{1}{2}(\gamma_s^1 + \gamma_s^2){Q_s}^2\right] \mp \frac{1}{2}\sqrt{\left[(E_1^0 - E_2^0) + \frac{1}{2}(\gamma_s^1 - \gamma_s^2){Q_s}^2\right]^2 + 4(\lambda_s^{1-2})^2 {Q_s}^2}, \tag{13}$$

where V_1 and V_2 are the lower and upper adiabatic potentials. It is seen from panels (a) and (c) of Fig. 4 that a strong interstate coupling is mediated through the ν_{10} vibrational modes in the $1^1\tilde{B}_u$–$1^1\tilde{B}_g$ and $1^1\tilde{B}_u$–$2^1\tilde{B}_g$ coupled surfaces. As a result, the lower $1^1\tilde{B}_u$ state has a double well shape (for more information, see Ref. 60) [cf. panels (a) and (c) of Fig. 4], while the upper $1^1\tilde{B}_g$ [cf. panel (a) of Fig. 4] and $2^1\tilde{B}_g$ [cf. panel (c) of Fig. 4] states become steeper. A clearer view of the topology of the lower surfaces is shown in the insets of panels (a) and (c) of Fig. 4. Similarly, the topological changes of the upper and lower PECs of the $1^1\tilde{B}_u$–$2^1\tilde{B}_g$ coupled surfaces due to the interstate

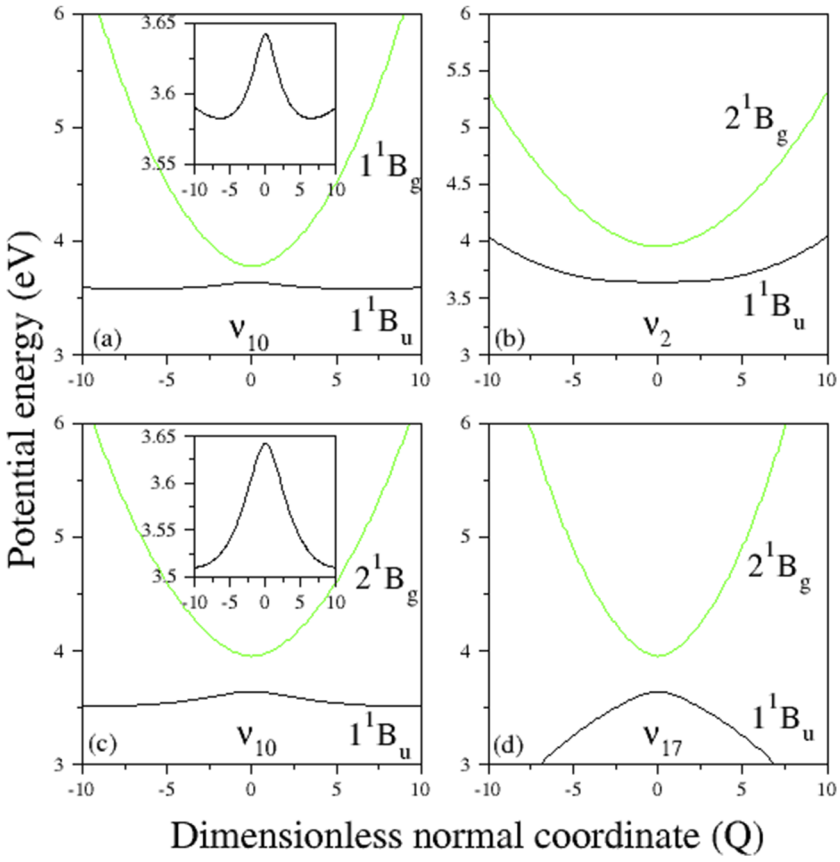

FIG. 4. Potential energy curves (PECs) of 1^1B_u, 1^1B_g, and 2^1B_g states, including interstate coupling between them along some selected non-totally symmetric normal coordinates of CPD. Selection of vibrational modes is performed considering their coupling strength between two electronic states $\left[\left(\frac{(\lambda^{j-k})^2}{2\omega_i^2}\right)\right]$; see Table V. PECs of 1^1B_u and 1^1B_g states along the ν_{10} vibrational mode are shown in (a), and the PECs between 1^1B_u and 2^1B_g states along ν_2, ν_{10}, and ν_{17} vibrational modes are shown in (b), (c), and (d), respectively.

coupling mediated via the ν_2 and ν_{17} vibrational modes are shown in panels (b) and (d) of Fig. 4.

The above discussions on the PECs of DHP and CPD indicate a possibility of a relatively simpler topology of the PESs of DHP, whereas the topology of the PESs of the electronic states of CPD is highly complex and coupled. The existence of several close lying CIs and energy minima of the electronic states will complicate the dynamics of CPD, especially in the case of high intrastate and interstate couplings. The continuation of the above discussion about the PECs in order to examine the role of vibronic coupling mediated simultaneously through one totally symmetric and one non-totally symmetric mode in the coupled PESs of CPD is elaborately discussed in the supplementary material, and the corresponding potential energy diagrams are presented in Fig. S3 of the supplementary material.

B. Vibronic structure of the absorption band of DHP and CPD

1. Vibronic structure on the uncoupled states

In this subsection, we first discuss about the Poisson spectral intensity distributions for selected totally symmetric vibrational modes. The Poisson intensity distribution $[P_k(E)]$[28,62–65] of the kth vibrational mode of an electronic state can be written as

$$P_k(E) = \sum_v \frac{a^v}{v!} \exp(-a)\delta(E - E_0 + a\omega - v\omega), \tag{14}$$

where $a = \frac{\kappa^2}{2\omega^2}$ is the Huang–Rhys parameter or Poisson parameter and v is a vibrational quantum number of a given vibrational mode. The values of the Huang–Rhys parameter of the vibrational modes of CPD are quite large compared to those for DHP. As a result, excitations to higher quantum levels of vibrational modes of CPD are expected for optically bright excited states. Poisson intensity distributions in the vibrational quantum levels of two strong Condon active modes for each optically bright excited state of DHP and CPD are examined, and the results are represented in Figs. 5 and 6, respectively. Figures 5 and 6 indicate rather wide Poisson intensity distributions for the excited states of CPD, while the intensity distributions for DHP are quite narrow. The diagrams represented in Fig. 5 indicate that the highest level of vibrational excitation in DHP is $v = 2$ and that the spectral intensities of the active vibrational modes are gradually decreasing when going from the fundamentals to their overtones. The diagrams represented in Fig. 6 indicate a quite different scenario. For example, for ν_4, which is the strongest Condon active vibrational mode in the optically bright excited states of CPD, the highest spectral intensity is found at vibrational levels 13, 1, and (2,3) in the $1^1\tilde{B}_u$, $1^1\tilde{A}_u$, and $2^1\tilde{B}_u$ state, respectively [cf. panels (a), (c), and (e) of Fig. 6]. Additional information concerning

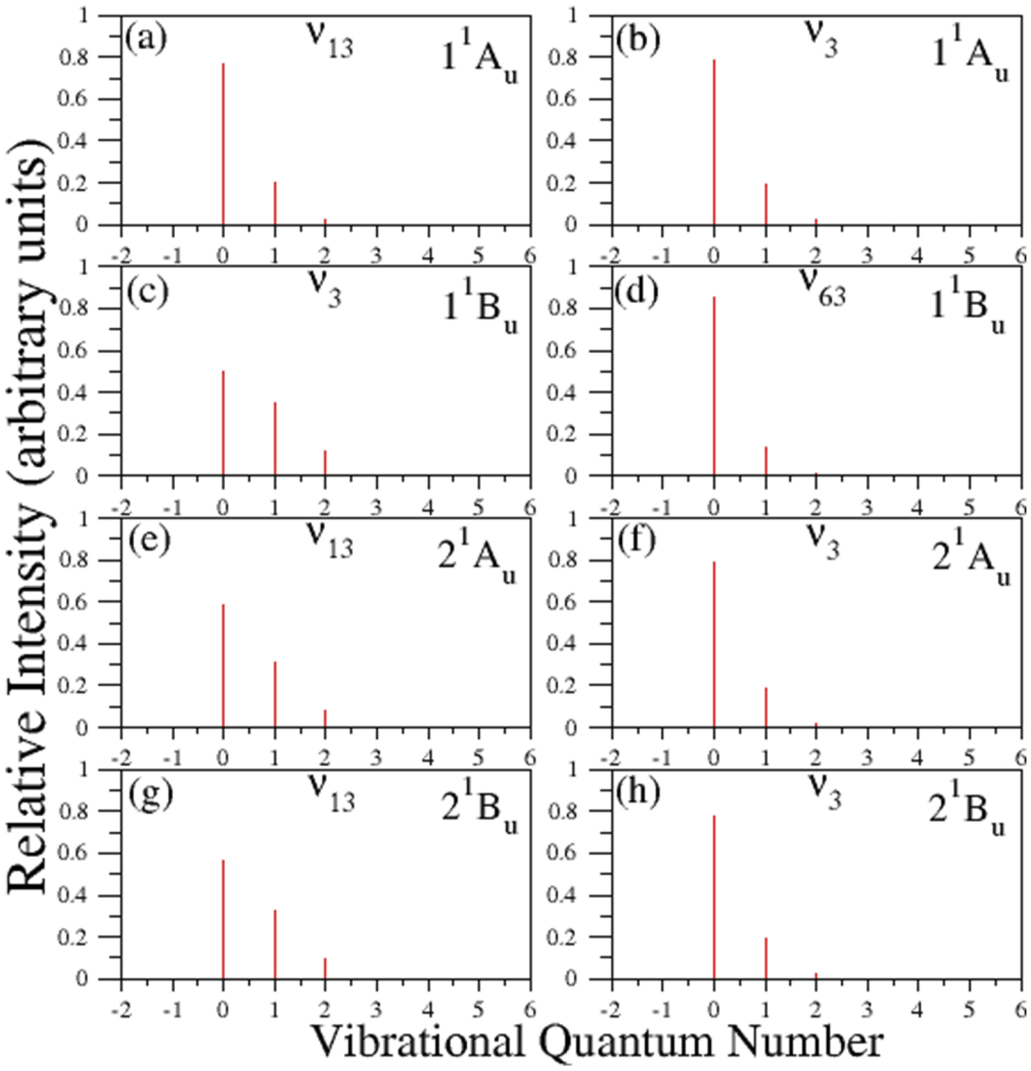

FIG. 5. Poisson intensity distributions (PIDs) in the vibrational quantum levels of vibrational modes of DHP possessing highest values of excitation strength in the $1^1\tilde{A}_u$, $1^1\tilde{B}_u$, $2^1\tilde{A}_u$, and $2^1\tilde{B}_u$ states. PIDs in the $1^1\tilde{A}_u$ state along ν_{13} and ν_3 vibrational modes are shown in (a) and (b), respectively. PIDs in the $1^1\tilde{B}_u$ state along ν_3 and ν_{63} vibrational modes are shown in (c) and (d), respectively. PIDs in the $2^1\tilde{A}_u$ state along ν_{13} and ν_3 vibrational mode are shown in (e) and (f), respectively. PIDs in the $2^1\tilde{B}_u$ state along ν_{13} and ν_3 vibrational modes are shown in (g) and (h), respectively.

the highest intensity in the Poisson distributions is given in Table SVIII of the supplementary material, and the data of Table SVIII indicate a vibrational congestion at least for the first optically bright excited state (i.e., $1^1\tilde{B}_u$) of CPD.

The uncoupled absorption spectra obtained through the TI formalism for the optically bright excited states of DHP and CPD are represented in Fig. 7. The spectra of panel (a) of Fig. 7 are obtained by including the most important ν_3, ν_{11}, ν_{13}, ν_{21}, ν_{22}, ν_{32}, and ν_{79} totally symmetric vibrational modes of DHP using a HO basis of 11, 9, 9, 5, 6, 5, and 8 functions, respectively, while the spectra of panel (b) of Fig. 7 are obtained by including the most important ν_4, ν_{12}, ν_{15}, ν_{21}, ν_{44}, ν_{55}, and ν_{67} totally symmetric vibrational modes of CPD, considering a HO basis of 20, 14, 14, 12, 10, 10, and 10 functions. Larger HO bases are used for the spectra simulations of CPD considering the higher excitations of the individual vibrational modes as discussed above. The spectra shown in Fig. 7 indicate a wider distribution of spectral intensities in the $1^1\tilde{B}_u$ state of CPD [cf. black spectra in panel (b) of Fig. 7] compared to the other absorption bands of both DHP and CPD, which is in accordance with the Poisson intensity distribution of the individual vibrational modes. These spectra also indicate possible vibrational energy level mixing between the $1^1\tilde{A}_u$ and $2^1\tilde{B}_u$ states of CPD [cf. red and blue spectra

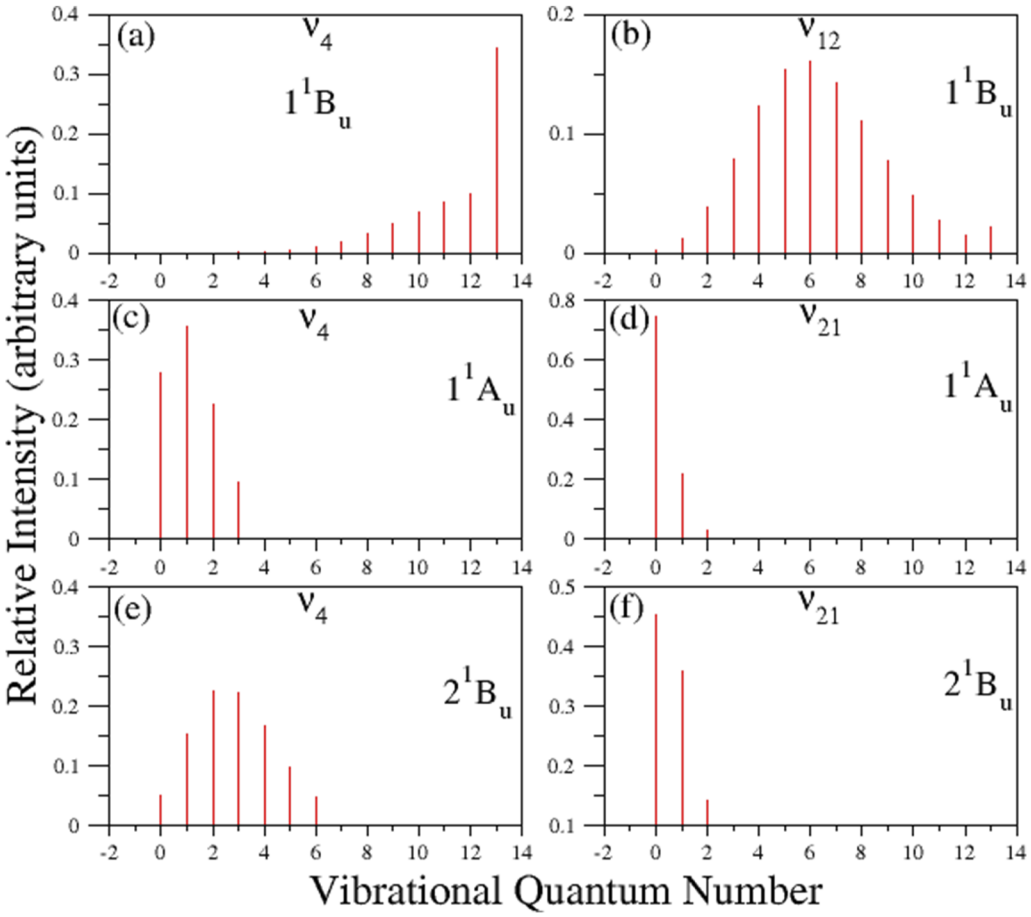

FIG. 6. Poisson intensity distributions (PIDs) in the vibrational quantum levels of vibrational modes of CPD possessing highest values of excitation strength in the $1^1\tilde{B}_u$, $1^1\tilde{A}_u$, and $2^1\tilde{B}_u$ states. PIDs in the $1^1\tilde{B}_u$ state along ν_4 and ν_{12} vibrational modes are shown in (a) and (b), respectively. PIDs in the $1^1\tilde{A}_u$ state along ν_4 and ν_{21} vibrational modes are shown in (c) and (d), respectively. PIDs in the $2^1\tilde{B}_u$ state along ν_4 and ν_{21} vibrational modes are shown in (e) and (f), respectively.

of panel (b) in Fig. 7], a feature that is completely missing in the case of DHP [cf. panel (a) of Fig. 7]. This occurs due to the presence of quasi-degeneracy between the $1^1\tilde{A}_u$–$2^1\tilde{B}_u$ CI and the energy minimum of the $2^1\tilde{B}_u$ state of CPD (cf. Table VI), which allows us to anticipate a possible population flow between these states. It is noted that the spectra represented in Fig. 7 are generated without oscillator-strength weighting.

We assigned some vibrational progressions in the four uncoupled absorption bands of DHP. The assignment of the vibronic energy levels of different states of DHP is performed by wavepacket (WP) density plots using the block-improved relaxation method[44,66,67] as implemented in the MCTDH program module.[42] The WP density plots of the vibronic energy level of $1^1\tilde{A}_u$, $1^1\tilde{B}_u$, $2^1\tilde{A}_u$, and $2^1\tilde{B}_u$ states of DHP are represented in Figs. S4–S7 of the supplementary material, respectively. The detailed protocol of the assignment of the vibronic energy levels can be found elsewhere.[65,68–71] The locations of the fundamentals of (ν_3, ν_{11}, and ν_{13}), (ν_3, ν_{11}, ν_{13}, ν_{22}, ν_{21}, and ν_{32}), (ν_3, ν_{11}, ν_{13}, ν_{22}, and ν_{32}), and (ν_3, ν_{11}, ν_{13}, ν_{22}, ν_{21}, and ν_{32}) are found at ~(169, 325, and 388 cm^{-1}), (165, 334, 381, 512, 556, and 777 cm^{-1}), (160, 331, and 385 cm^{-1}), and (162, 318, 391, 511, 554, and 753 cm^{-1}) from the 0_0^0 line of $1^1\tilde{A}_u$, $1^1\tilde{B}_u$, $2^1\tilde{A}_u$, and $2^1\tilde{B}_u$ states, respectively. The above assignments are performed by observing one nodal plane along the corresponding normal coordinate, and the respective WP density plots of the above-mentioned vibronic energy lines in the $1^1\tilde{A}_u$, $1^1\tilde{B}_u$, $2^1\tilde{A}_u$, and $2^1\tilde{B}_u$ state of DHP are shown in panels (a), (b), and (d) of Fig. S4; panels (a), (c), (d), (g), (h), and (i) of Fig. S5; panels (a), (c), (d), (g), and (i) of Fig. S6; and panels (a)–(c), (e), (g), and (h) of Fig. S7. Similarly, the assignment of the first overtone and the combination peak is performed by observing two nodal planes and simultaneous nodal planes along the corresponding normal coordinate. The first overtone of ν_3 is found to be ~339 cm^{-1} [cf. panel (c) in Fig. S4 of the supplementary material], ~331 cm^{-1} [cf. panel (b) in Fig. S5 of the supplementary material], and ~321 cm^{-1} [cf. panel (b) in Fig. S6 of the supplementary material] in the $1^1\tilde{A}_u$, $1^1\tilde{B}_u$, and $2^1\tilde{A}_u$ state, respectively. It is also found from these plots that ν_3, ν_{11}, ν_{13}, and ν_{79} vibrational modes

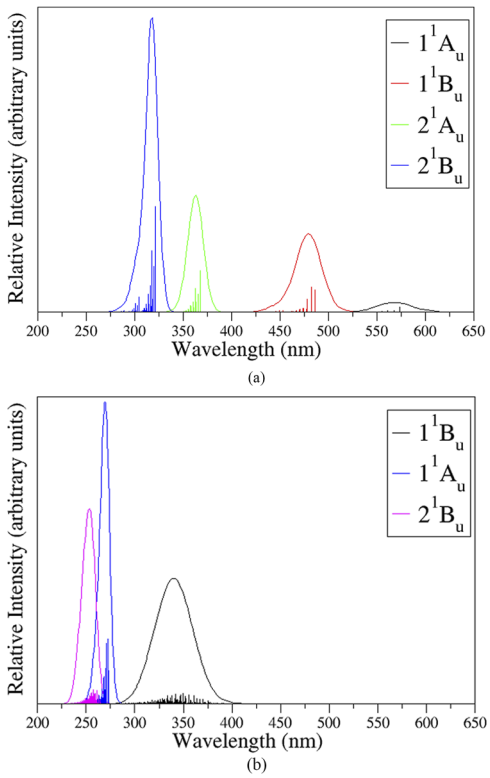

FIG. 7. Overall uncoupled spectra of $1^1\tilde{A}_u$, $1^1\tilde{B}_u$, $2^1\tilde{A}_u$, and $2^1\tilde{B}_u$ states of DHP (a) and $1^1\tilde{B}_u$, $1^1\tilde{A}_u$, and $2^1\tilde{B}_u$ states of CPD (b). The spectra are obtained using the parameters of Tables II–IV. The stick lines are generated from matrix diagonalization, and the envelope of each spectrum is obtained by convoluting the stick lines with the Lorentzian function using 0.087 eV full-width at half-maximum (FWHM). Time-independent calculations are performed with seven important totally symmetric vibrational modes, ν_3, ν_{11}, ν_{13}, ν_{21}, ν_{22}, ν_{32}, and ν_{79}, and four electronic states for DHP. The same calculations for CPD are performed with seven important totally symmetric vibrational modes, ν_4, ν_{12}, ν_{15}, ν_{21}, ν_{44}, ν_{55}, and ν_{67}, and three optically bright states.

are very likely to form combination peaks between them and also with other vibrational modes in the four excited states of DHP.

Similarly, we assign the fundamental vibrational progression of ν_{15}, ν_{21}, and ν_{67} at ~423, 524, and 1441 cm^{-1}, respectively, from the 0_0^0 line at the $1^1\tilde{B}_u$ state [cf. panels (a)–(c), respectively, in Fig. S8 of the supplementary material]. The fundamental of ν_4 and ν_{21} and the first overtone of ν_4 in the $1^1\tilde{A}_u$ state are found at ~144, 499, and 288 cm^{-1} from the 0_0^0 line at the $1^1\tilde{A}_u$ state [cf. panels (d), (f), and (e), respectively, in Fig. S8 of the supplementary material]. The fundamental of ν_{15}, ν_{21}, and ν_{67} in the $2^1\tilde{B}_u$ state are found at ~427, 508, and 938 cm^{-1}, respectively, from the 0_0^0 line at the $2^1\tilde{B}_u$ state [cf. panels (g)–(i), respectively, in Fig. S8 of the supplementary material].

2. Vibronic structure on the coupled states: Impact of electronic non-adiabatic coupling

The impact of non-adiabatic coupling in conjunction with CIs between the first four excited states of DHP and the first five excited states of CPD is examined on the basis of TD quantum dynamics as implemented in MCTDH program.[42] A TI calculation (matrix diagonalization) cannot be performed owing to a huge increase of dimensionality resulting from the inclusion of non-totally symmetric modes.

The overall vibronic band structure obtained from the four coupled state ($1^1\tilde{A}_u$–$1^1\tilde{B}_u$–$2^1\tilde{A}_u$–$2^1\tilde{B}_u$) calculations of DHP is represented in panel (b) of Fig. 8, indicated by the black solid line, and the result is compared with the available experimental spectrum reproduced from Ref. 36 in panel (a) of Fig. 8. Four distinct absorption bands are obtained in accordance with the existence of well-separated PECs (cf. Fig. 2) and weak intrastate couplings (cf. Table III), as discussed above. In addition, the estimation of the energetic locations of the CIs and state minimum (cf. Table VI) indicates significant energy gaps between the CIs and the minimum of the upper electronic state, except the energy gap between the $1^1\tilde{A}_u$–$1^1\tilde{B}_u$ CI and energy minimum of the $1^1\tilde{B}_u$ state. The combined effects of the moderate interstate couplings between $1^1\tilde{A}_u$ and $1^1\tilde{B}_u$ states (see Table V) and the low energy gap between the $1^1\tilde{A}_u$–$1^1\tilde{B}_u$ CI and energy minimum of $1^1\tilde{B}_u$ state (cf. Table VI) initiate the non-adiabatic effects between these states. This causes the electronic population flow between these states (cf. Fig. S9 of the supplementary material). A moderate interstate couplings exist between the other states of DHP, but the existence of a high energy gap between the CI and the energy minimum of the upper state prohibits the non-adiabatic effects between the other states of DHP. That is why, one cannot find the electronic population flow between the other states of DHP.

It can be seen from our previous *FC_Class* [see Fig. 2(a) in Ref. 36] and nuclear ensemble (NE) (see Fig. 5 in Ref. 36) simulations that the hump of the second absorption band of DHP (i.e., $1^1A_g \rightarrow 1^1B_u$ electronic transition) was not generated as one can find it in the experimental observation [see Fig. 1 in Ref. 36 and Fig. 8(a)], while the previous *FC_Class* [see Fig. 2(a) in Ref. 36] simulations of the third absorption band of DHP (i.e., $1^1A_g \rightarrow 2^1A_u$ electronic transition) were not in order to the experimental observation [see Fig. 1 in Ref. 36 and Fig. 8(a)] with regard to hump generation, and NE simulations of the same absorption band of DHP showed resemblance with the experimental observation by not generating the hump. In case of a fourth absorption band of DHP (i.e., $1^1A_g \rightarrow 2^1A_u$ electronic transition), NE simulations did not produce any hump, while *FC_Class* simulations produced one hump, which was in partial resemblance with the experimental observation of two humps of the corresponding absorption band. In this context, the comparison of our calculated absorption spectra [cf. Fig. 8(b)] in the present study and the experimental findings of Ref. 36 indicates a quite good accordance, specially concerning the shape of the spectra. The vibronic simulations of the present study produce the hump of the second absorption band, while those produce the third absorption band without hump. On the other hand, the present vibronic simulations also produce one hump in the fourth absorption band of DHP.

It is expected that the good agreement of the present vibronic simulations with the experimental observations of the absorption band of DHP occurs due to the consideration of the non-adiabatic effects in the present study. In order to confirm our hypothesis, we simulate the absorption spectra of DHP, including only the totally symmetric vibrational modes, which are included in the coupled

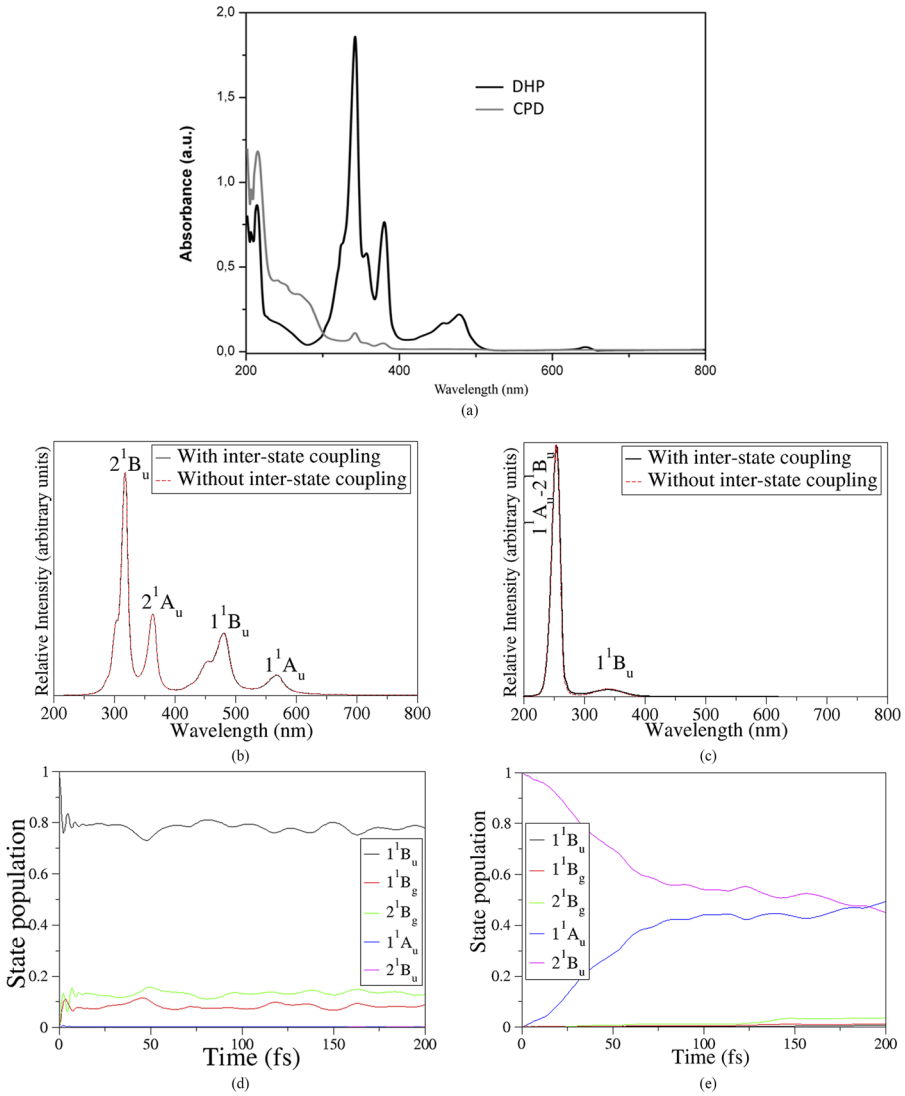

FIG. 8. Comparison between experimental[36] (a) and vibronically coupled absorption spectra of DHP (b) and CPD (c). The experimental spectra were recorded for the methyl substituted DHP and CPD. The vibronic structure of the absorption bands of DHP shown in (b) is obtained from the $1^1\tilde{A}_u$–$1^1\tilde{B}_u$–$2^1\tilde{A}_u$–$1^1\tilde{B}_u$ coupled states time-dependent nuclear dynamics, including 18 vibrational modes listed in Table I, while the same for CPD shown in (c) is obtained from the $1^1\tilde{B}_u$–$1^1\tilde{B}_g$–$2^1\tilde{B}_g$–$1^1\tilde{A}_u$–$2^1\tilde{B}_u$ coupled state time-dependent nuclear dynamics, including 20 vibrational modes listed in Table I. The diabatic electronic population of the five excited states of CPD is shown in (d) and (e), while the initial WP is prepared on the $1^1\tilde{B}_u$ and $2^1\tilde{B}_u$ state, respectively.

state calculation, and the result of this calculation is represented in panel (b) of Fig. 8, indicated by a red dashed line. The superimposition of these two spectra, adiabatic (red dashed line) and coupled (black solid line), indicates that the non-adiabatic effects play a very minor role in the simulation of the absorption spectra of DHP. The present findings are also in accordance with our previous findings of *FC_Class*[36] simulations, especially for $1^1A_g \rightarrow 2^1A_u$ electronic transition.

In contrast to the DHP, the dynamics of CPD is likely to be more affected by non-adiabatic coupling. The interstate couplings between the $1^1\tilde{B}_u$ and $1^1\tilde{B}_g$ and $2^1\tilde{B}_g$ states (cf. Table V) and the intrastate couplings of the $1^1\tilde{B}_u$ (cf. Table IV) state of CPD are quite high. Therefore, we have seen that the topology of the bright $1^1\tilde{B}_u$ state is highly affected by the presence of the energetically close optically dark $1^1\tilde{B}_g$ and $2^1\tilde{B}_g$ states (cf. Fig. 4 and Fig. S3 of the supplementary material). We first consider the absorption spectra obtained from the nuclear dynamics without oscillator-strength weighting both on the coupled and on the uncoupled states of CPD in Fig. S10 of the supplementary material, indicated by the black solid line and red dashed line, respectively. The electronic population flow between states is shown in panels (d) and (e) of Fig. 8 when the initial WP is put on the $1^1\tilde{B}_u$ and $2^1\tilde{B}_u$ state, respectively. The absorption spectra shown in Fig. S10 of the supplementary material indicate a spectral broadening of the first coupled absorption band (specially at the 280–320 nm and near 400 nm) as compared to the spectrum obtained from uncoupled formalism. This might occur due to the non-adiabatic decay of the electronic population of the $1^1\tilde{B}_u$ state toward its adjacent optically dark states [cf. panel (d) of Fig. 8]. The spectral broadening of the second coupled absorption band of CPD, specially the $2^1\tilde{B}_u$ band, occurs due to the electronic population transfer from the $2^1\tilde{B}_u$ state to the $1^1\tilde{A}_u$ state, as shown in panel (e) of Fig. 8. The quasi-degeneracy of the

$1^1\tilde{A}_u$–$2^1\tilde{B}_u$ CI and the minimum of the $2^1\tilde{B}_u$ state of CPD initiates vibronic energy flow from the $2^1\tilde{B}_u$ state to $1^1\tilde{A}_u$ state, while the existence of low interstate couplings between $1^1\tilde{A}_u$ and $2^1\tilde{B}_u$ states (cf. Table V) and quite low energetic location of the minimum of the $1^1\tilde{A}_u$ state as compared to the energetic location of the $1^1\tilde{A}_u$–$2^1\tilde{B}_u$ CI (~0.1 eV) inhibits the perturbation of the vibronic levels near the energy minimum of $1^1\tilde{A}_u$ state. As a result, an immediate reverse population flow to the $2^1\tilde{B}_u$ state from the $1^1\tilde{A}_u$ state cannot be observed (see Fig. S11 of the supplementary material). The oscillator-strength weighted calculated absorption spectra of CPD from the nuclear dynamics on both the uncoupled and coupled surfaces are shown in panel (c) of Fig. 8 with the red and black line, respectively. The band shape of these spectra is quite different from the spectra without including oscillator-strength weighting presented in Fig. S10 of the supplementary material. The relative intensity of the first absorption band of CPD at ~350 nm region presented in panel (c) of Fig. 8 is quite suppressed as compared to the one presented in Fig. S10 of the supplementary material due to the approximately 20 time lower oscillator strength (cf. Table II) of $1^1\tilde{B}_u$ as compared to the oscillator strength of the $2^1\tilde{B}_u$ state. As a result, the difference between the uncoupled and coupled spectra of CPD represented in panel (c) of Fig. 8 is not prominent. Moreover, the intensity of the absorption band obtained from $1^1\tilde{A}_u$ is totally suppressed by the oscillator-strength weighting due to its very low value (cf. Table II). Hence, the contribution to the overall intensity comes from the $2^1\tilde{B}_u$ state for the second band of CPD represented in panel (c) of Fig. 8.

IV. SUMMARY AND OUTLOOK

The present theoretical study is primarily devoted to the description of the absorption band structure of the photochromic DHP/CPD couple employing vibronic coupling theory. This study is based on the construction of two separate molecular Hamiltonians for DHP and CPD, including the first four and first five excited electronic states, respectively. The expansion of the Hamiltonian's elements is determined by fits of the analytic form of the potential to the TD-DFT energy points. The detailed topology of the one-dimensional adiabatic potential energy curves along totally symmetric and non-totally symmetric vibrational modes is examined. Later, the topological change of the coupled potential energy surfaces due to the dual activity of tuning of energy separation between two electronic states and interstate coupling between those states are also examined considering the simultaneous presence of totally and non-totally symmetric vibrational modes. Following the analyses of the electronic structures, we first calculate the Poisson intensity distribution of the individual vibrational modes in the individual electronic states. The main finding of this study is that the Poisson intensity is highly distributed among the vibrational levels for CPD. Later, time-independent calculations on the uncoupled PES, including the active totally symmetric vibrational modes, indicate the possibility of vibrational energy flow from the $2^1\tilde{B}_u$ state to the $1^1\tilde{A}_u$ state of CPD through $1^1\tilde{A}_u$–$2^1\tilde{B}_u$ CI. We find that the results of both the adiabatic and non-adiabatic simulations using the time-dependent approach are consistent with the four absorption bands of DHP observed experimentally. In contrast, the present study shows that the non-adiabatic transitions play a more important role for CPD. The coupling between the bright $1^1\tilde{B}_u$ state and the optically dark $1^1\tilde{B}_g$ and $2^1\tilde{B}_g$ excited electronic states plays a crucial role in the generation of the first band of CPD. On the other side, the significant population transfer between the $2^1\tilde{B}_u$ state and the $1^1\tilde{A}_u$ state occurring via an easily accessible low-lying CI between these states plays a pivotal role in the formation of the second band of CPD.

The present study shows that TD-DFT provides a reasonable electronic structure method for the computation of the excited states relevant to the absorption properties of the DHP/CPD photochromic couple, and the simulated absorption bands obtained from these electronic structures are in good agreement with the experimental findings. On the other hand, the influence of close-lying singlet excited states ($2^1\tilde{A}_g$ and $1^1\tilde{B}_g$ for DHP and $2^1\tilde{A}_g$ and $2^1\tilde{A}_u$ for CPD) of double electronic excitations in nature is missing in the present study as standard TD-DFT is not suitable for the electronic structure calculations of doubly excited states. Moreover, the influence of pure electronic couplings due to the presence of the same symmetry states (for example, $1^1\tilde{A}_u$–$2^1\tilde{A}_u$ and $1^1\tilde{B}_u$–$2^1\tilde{B}_u$ coupling for DHP and $1^1\tilde{B}_u$–$2^1\tilde{B}_u$ and $1^1\tilde{B}_g$–$2^1\tilde{B}_g$ coupling for CPD) is also missing from the present calculations. Inclusion of the above-mentioned effects would require using more sophisticated electronic structure methods and an extension of the vibronic coupling Hamiltonians. Future exciting work could also involve the extension of such a vibronic coupling Hamiltonian model to study larger amplitude motions of the nuclei involved in the early steps of the DHP to CPD photoisomerization.

SUPPLEMENTARY MATERIAL

See the supplementary material for the PECs generated from the simultaneous effects of totally symmetric and non-totally symmetric vibrational modes of CPD, a complete set of data regarding parameters of Hamiltonians of DHP and CPD, the primitive and SPF basis of dynamical calculations, vibrational quantum numbers, displacement vectors for normal modes included in the dynamics of DHP and CPD, assignments for vibronic energy levels, transfer of diabatic electronic population, and absorption bands of CPD without considering oscillator strengths.

ACKNOWLEDGMENTS

This work was granted access to the HPC resources of the CALMIP supercomputing center under allocation 2018-[12158]. We acknowledge the LABEX NanoX for funding R. Sarkar's post-doctoral fellowship (EUR Grant NanoX No. ANR-17-EURE-0009). We also acknowledge the financial support from the Agence Nationale de la Recherche through Grant No. ANR-18-CE29-0012 (Photochromics project). We thank Dr. F. X. Gadéa for many fruitful discussions.

AUTHOR DECLARATIONS

Conflict of Interest

The authors have no conflicts to disclose.

Author Contributions

Rudraditya Sarkar: Conceptualization (equal); Data curation (equal); Formal analysis (equal); Investigation (equal); Methodology

(equal); Project administration (equal); Software (equal); Validation (equal); Visualization (equal); Writing – original draft (equal); Writing – review & editing (equal). **Marie-Catherine Heitz**: Data curation (equal); Formal analysis (equal); Methodology (equal); Resources (equal); Validation (equal); Visualization (equal); Writing – review & editing (equal). **Martial Boggio-Pasqua**: Data curation (equal); Formal analysis (equal); Funding acquisition (equal); Investigation (equal); Project administration (equal); Resources (equal); Software (equal); Supervision (equal); Validation (equal); Visualization (equal); Writing – review & editing (equal).

DATA AVAILABILITY

The data that support the findings of this study are available within the article and its supplementary material.

REFERENCES

[1] H.-R. Blattmann, D. Meuche, E. Heilbronner, R. J. Molyneux, and V. Boekelheide, J. Am. Chem. Soc. **87**, 130 (1965).
[2] V. Boekelheide and J. B. Phillips, Proc. Natl. Acad. Sci. U. S. A. **51**, 550 (1964).
[3] V. Boekelheide and J. B. Phillips, J. Am. Chem. Soc. **89**, 1695 (1967).
[4] L. Ordronneau, H. Nitadori, I. Ledoux, A. Singh, J. A. G. Williams, M. Akita, V. Guerchais, and H. Le Bozec, Inorg. Chem. **51**, 5627 (2012).
[5] T. Nakagawa, Y. Hasegawa, and T. Kawai, Chem. Commun. **2009**, 5630.
[6] M. Morimoto, H. Miyasaka, M. Yamashita, and M. Irie, J. Am. Chem. Soc. **131**, 9823 (2009).
[7] A. Athanassiou, M. I. Lygeraki, D. Pisignano, K. Lakiotaki, M. Varda, E. Mele, C. Fotakis, R. Cingolani, and S. H. Anastasiadis, Langmuir **22**, 2329 (2006).
[8] B. Xin and J. Hao, J. Chem. Soc. Rev. **39**, 769 (2010).
[9] S. Lara-Avila, A. V. Danilov, S. E. Kubatkin, S. L. Broman, C. R. Parker, and M. B. Nielsen, J. Phys. Chem. C **115**, 18372 (2011).
[10] S. J. van der Molen, J. Liao, T. Kudernac, J. S. Agustsson, L. Bernard, M. Calame, B. J. van Wees, B. L. Feringa, and C. Schönenberger, Nano Lett. **9**, 76 (2009).
[11] H.-R. Blattmann and W. Schmidt, Tetrahedron **26**, 5885 (1970).
[12] W. Schmidt, Helv. Chim. Acta **54**, 862 (1971).
[13] W. Schmidt, Tetrahedron Lett. **13**, 581 (1972).
[14] S.-I. Murakami, T. Tsutsui, S. Saito, T. Yamato, and M. Tashiro, Nippon Kagaku Kaishi **221**, 221–229 (1988).
[15] R. S. Murphy, Y. Chen, T. R. Ward, R. H. Mitchell, and C. Bohne, Chem. Commun. **1999**, 2097.
[16] M. A. L. Sheepwash, R. H. Mitchell, and C. Bohne, J. Am. Chem. Soc. **124**, 4693 (2002).
[17] R. H. Mitchell, T. R. Ward, Y. Chen, Y. Wang, S. A. Weerawarna, P. W. Dibble, M. J. Marsella, A. Almutairi, and Z.-Q. Wang, J. Am. Chem. Soc. **125**, 2974 (2003).
[18] S. G. Robinson, V. A. Sauro, and R. H. Mitchell, J. Org. Chem. **74**, 6592 (2009).
[19] D. Roldan, S. Cobo, F. Lafolet, N. Vilà, C. Bochot, C. Bucher, E. Saint-Aman, M. Boggio-Pasqua, M. Garavelli, and G. Royal, Chem. - Eur. J **21**, 455 (2015).
[20] R. V. Williams, W. D. Edwards, R. H. Mitchell, and S. G. Robinson, J. Am. Chem. Soc. **127**, 16207 (2005).
[21] M. Boggio-Pasqua, M. J. Bearpark, and M. A. Robb, J. Org. Chem. **72**, 4497 (2007).
[22] M. Boggio-Pasqua and M. Garavelli, J. Phys. Chem. A **119**, 6024 (2015).
[23] K. Klaue, Y. Garmshausen, and S. Hecht, Angew. Chem., Int. Ed. **57**, 1414 (2018).
[24] M. Jacquet, L. M. Uriarte, F. Lafolet, M. Boggio-Pasqua, M. Sliwa, F. Loiseau, E. Saint-Aman, S. Cobo, and G. Royal, J. Phys. Chem. Lett. **11**, 2682 (2020).
[25] L. Han, H. Li, X. Zuo, Q. Gao, D. Li, B. Cui, C. Fang, and D. Liu, Phys. Chem. Chem. Phys. **22**, 26255 (2020).
[26] K. Klaue, W. Han, P. Liesfeld, F. Berger, Y. Garmshausen, and S. Hecht, J. Am. Chem. Soc. **142**, 11857 (2020).
[27] Z. Ziani, F. Loiseau, E. Lognon, M. Boggio-Pasqua, C. Philouze, S. Cobo, and G. Royal, Chem. - Eur. J **27**, 16642 (2021).
[28] H. Köppel, W. Domcke, and L. S. Cederbaum, Adv. Chem. Phys. **57**, 59 (1984).
[29] L. S. Cederbaum, W. Domcke, and H. Köppel, Chem. Phys. Lett. **33**, 319 (1978).
[30] W. Domcke, H. Köppel, and L. S. Cederbaum, Mol. Phys. **43**, 851 (1981).
[31] H. Köppel, L. S. Cederbaum, and W. Domcke, Chem. Phys. **69**, 175 (1982).
[32] W. Domcke, D. R. Yarkony, and H. Köppel, *Conical Intersections: Electronic Structure, Dynamics and Spectroscopy* (World Scientific, Singapore, 2004).
[33] S. Mahapatra, Acc. Chem. Res. **42**, 1004 (2009).
[34] S. Mahapatra, Wiley Interdiscip. Rev.: Comput. Mol. Sci. **12**, e1576 (2022).
[35] M. A. L. Sheepwash, T. R. Ward, Y. Wang, S. Bandyopadhyay, R. H. Mitchell, and C. Bohne, Photochem. Photobiol. Sci. **2**, 104 (2003).
[36] R. Sarkar, M.-C. Heitz, G. Royal, and M. Boggio-Pasqua, J. Phys. Chem. A **124**, 1567 (2020).
[37] H.-D. Meyer, U. Manthe, and L. S. Cederbaum, Chem. Phys. Lett. **165**, 73 (1990).
[38] U. Manthe, H. D. Meyer, and L. S. Cederbaum, J. Chem. Phys. **97**, 3199 (1992).
[39] M. H. Beck and H.-D. Meyer, Z. Phys. D: At., Mol. Clusters **42**, 113 (1997).
[40] M. H. Beck, A. Jäckle, G. A. Worth, and H.-D. Meyer, Phys. Rep. **324**, 1 (2000).
[41] H.-D. Meyer and G. A. Worth, Theor. Chem. Acc. **109**, 251 (2003).
[42] M. H. Beck, A. Jäckle, G.A. Worth, and H.-D. Meyer, The mctdh package, Version 8.4.15, University of Heidelberg, Heidelberg, Germany. See http://mctdh.uni-hd.de.
[43] H.-D. Meyer, J. Phys.: Conf. Ser. **4**, 66 (2005).
[44] L. J. Doriol, F. Gatti, C. Lung, and H.-D. Meyer, J. Chem. Phys. **129**, 224109 (2008).
[45] P. A. M. Dirac, Proc. Cambridge Philos. Soc. **26**, 376 (1930).
[46] J. Frenkel, *Wave Mechanics* (Clarendon, Oxford, 1934).
[47] M. Sala, B. Lasorne, F. Gatti, and S. Guérin, Phys. Chem. Chem. Phys. **16**, 15957 (2014).
[48] C. Lanczos, J. Res. Natl. Bur. Stand. **45**, 255 (1950).
[49] J. Cullum and R. Willoughby, *Lanczos Algorithms for Large Symmetric Eigenvalue Problems* (Birkhäuser, Boston, 1985), Vols. I and II.
[50] W. Domcke and H. Köppel, *Encyclopedia of Computational Chemistry*, edited by P.v.R. Schleyer (Wiley, New York, 1998), p. 3166.
[51] M. J. Frisch, G. W. Trucks, H. B. Schlegel, G. E. Scuseria, M. A. Robb, J. R. Cheeseman, G. Scalmani, V. Barone, B. Mennucci, G. A. Petersson, H. Nakatsuji, M. Caricato, X. Li, H. P. Hratchian, A. F. Izmaylov, J. Bloino, G. Zheng, J. L. Sonnenberg, M. Hada, M. Ehara, K. Toyota, R. Fukuda, J. Hasegawa, M. Ishida, T. Nakajima, Y. Honda, O. Kitao, H. Nakai, T. Vreven, J. A. Montgomery, Jr., J. E. Peralta, F. Ogliaro, M. Bearpark, J. J. Heyd, E. Brothers, K. N. Kudin, V. N. Staroverov, T. Keith, R. Kobayashi, J. Normand, K. Raghavachari, A. Rendell, J. C. Burant, S. S. Iyengar, J. Tomasi, M. Cossi, N. Rega, J. M. Millam, M. Klene, J. E. Knox, J. B. Cross, V. Bakken, C. Adamo, J. Jaramillo, R. Gomperts, R. E. Stratmann, O. Yazyev, A. J. Austin, R. Cammi, C. Pomelli, J. W. Ochterski, R. L. Martin, K. Morokuma, V. G. Zakrzewski, G. A. Voth, P. Salvador, J. J. Dannenberg, S. Dapprich, A. D. Daniels, O. Farkas, J. B. Foresman, J. V. Ortiz, J. Cioslowski, and D. J. Fox, GAUSSIAN 09, Revision D.01, Gaussian, Inc., Wallingford CT, 2013.
[52] A. D. Becke, J. Chem. Phys. **98**, 5648 (1993).
[53] E. B. Wilson, Jr., J. C. Decius, and P. C. Cross, *Molecular Vibrations* (McGraw-Hill, New York, 1995).
[54] T. Yanai, D. P. Tew, and N. C. Handy, Chem. Phys. Lett. **393**, 51 (2004).
[55] S. Matsika, J. Phys. Chem. A **108**, 7584 (2004).
[56] K. A. Kistler and S. Matsika, J. Phys. Chem. A **111**, 8708 (2007).
[57] S. Matsika, Rev. Comput. Chem. **23**, 83 (2007).
[58] S. Matsika and P. Krause, Annu. Rev. Phys. Chem. **62**, 621 (2011).
[59] Mathematica 8.0; Wolfram Research, Inc., System Modeler, Version 3.0, Champaign, IL, 2012.

[60]H. Köppel, L. S. Cederbaum, W. Domcke, and S. S. Shaik, Angew. Chem., Int. Ed. Engl. **22**, 210 (1983).
[61]R. Sarkar, J. Phys.: Conf. Ser. **759**, 012058 (2016).
[62]A. Kumar, T. R. Rao, and R. Sarkar, Phys. Chem. Chem. Phys. **23**, 3160 (2021).
[63]L. S. Cederbaum and W. Domcke, Adv. Chem. Phys. **36**, 205 (1977).
[64]A. B. Trofimov, H. Köppel, and J. Schirmer, J. Chem. Phys. **109**, 1025 (1998).
[65]A. Kumar, S. Agrawal, T. R. Rao, and R. Sarkar, Phys. Chem. Chem. Phys. **21**, 22359 (2019).
[66]R. Kosloff and H. Tal-Ezer, Chem. Phys. Lett. **127**, 223 (1986).
[67]H.-D. Meyer, F. L. Quéré, C. Léonard, and F. Gatti, Chem. Phys. **329**, 179 (2006).
[68]R. Sarkar and S. Mahapatra, J. Phys. Chem. A **120**, 3504 (2016).
[69]R. Sarkar and S. Mahapatra, J. Chem. Phys. **147**, 194305 (2017).
[70]R. Sarkar, S. Rajagopala Reddy, S. Mahapatra, and H. Köppel, Chem. Phys. **482**, 39 (2017).
[71]R. Sarkar, D. Baishya, and S. Mahapatra, Chem. Phys. **515**, 679 (2018).